DESIGN AND NOISE ANALYSIS OF AN OPERATIONAL AMPLIFIER-PHOTODIODE PAIR FOR USE IN FIBER OPTIC SENSORS

BY

THOMAS GARY WHITE

B.S. , University of Utah, 1985

THESIS

Submitted in partial fulfillment of the requirements
for the degree of Master of Science in Electrical Engineering
in the Graduate College of the
University of Illinois at Urbana-Champaign, 1987

Urbana, Illinois

ABSTRACT

A fluorescent dye coupled to the end of an optical fiber provides a sensor which is useful in measuring the concentration of specific compounds in solution. When the dye is excited by a light source, the fluorescent return is detected and provides information concerning the molecular interactions of the dye. In many cases the return light flux from the fluorescent dye is weak and special considerations must be taken to minimize the noise within the detection system. The noise present within the initial stage of detection and amplification is the dominant noise component of the system and care must be taken to choose the correct components. Furthermore, various techniques can be used to optimize the signal-to-noise ratio. The advantages of various detection schemes are discussed. A complete analysis of the frequency response, time domain behavior, noise characteristics and optimization techniques for a photodiode-operational amplifier pair is presented.

ACKNOWLEDGEMENTS

I am deeply grateful to those who have assisted in the completion of this project. I am especially thankful for the guidance and assistance provided by Professor Richard Magin. His insight and direction allowed me to narrow the scope of the project and complete it within the alloted time. I am also thankful for my co-workers John McCarthy, Kevin Ehlert and Dave Linstrom for their assistance and encouragement. I am grateful to Emad Ebbini for his willingness to allow me to run the programs and generate the necessary plots on the Cray XMP. I appreciate his taking time out of his busy schedule to assist. I am also grateful to all the others within the Bioacoustics Research Laboratory who have assisted in one way or another. These include Harold Underwood and Joe Cobb, who often assisted in technical matters, Billy McNeill, Wanda Elliott, Loralie Ma, Ben Tang and Jen Zhang.

I appreciate those who have not been directly involved with the project but have assisted in various ways. My roomates Andy Hull, Emmanuel Ramli and Irwan Halim have given technical advice, encouragement and have supported me in their prayers. I am especially thankful for my family, who have offered encouragement and support during the course of the project. Finally, I am thankful for the strength, patience and skills received from the Lord Jesus Christ, may this be to His glory.

TABLE OF CONTENTS

CHAPTER 1

INTRODUCTION

Advances in fluorescent chemistry have made possible the design and fabrication of new sensors which capitalize on the unique properties of fluorescent compounds. Fluorescent compounds, upon excitation, emit photons of one or more specific wavelengths. The emission wavelength is dependent on the properties and chemical interactions of the dye. When a fluorescent dye is placed in a solution, the chemical environment is changed, causing an alteration in the conformation or ionization of the dye. These changes are reflected in the spectral emission characteristics of the dye. Detection of the peak spectral emission of the dye following excitation can be used to investigate the characteristic properties of a solution.

A sensor consisting of a fluorescent dye immobilized at the end of a single optical fiber would be very useful for continuous in-vivo measurements. For example, the technique currently in use to measure the pH and blood gases (pCO_2, pO_2) is an in-vitro diagnostic laboratory. This requires blood to be removed from the patient and transferred to the diagnostic laboratory for evaluation. With the application of a fiber optic sensor containing a blood-gas specific fluorescent dye, the sensor could be inserted into the patient for an extended period of time, i.e., along with a catheter. This would allow a continuous status report of the blood gas

concentrations and any changes in blood gas levels could be readily detected. The continuous monitoring of blood gas changes would be beneficial in the diagnosis and treatment of conditions such as pulmonary or metabolic disorders.

Fiber optic sensors have many other advantages in physiological applications. The diameter of optical fibers is small, being on the order of 250 microns (0.25 mm) but can be less than 100 microns.[1] The small sizes are flexible, yet strong. Plastic fibers have a breaking strength of 1000 kg-cm^2, which is sufficiently strong for use in physiological applications. When the optical fiber is bent beyond the critical angle necessary for the complete internal reflection of the signal, there will be optical losses. This limits the flexibility of the fibers to some extent; however, for most applications, the flexibility is sufficient. Optical fibers are free from direct electrical contact and thereby safe in a clinical setting. The fibers are also free from any electrical noise present within the environment. Since electrical noise is not coupled to the optical signal, measurements in an environment with a large amount of electrical noise could effectively be linked by an optical fiber to a noiseless room with the necessary measurement equipment. The optical signal could then be converted to the electrical signal with a negligible light loss caused by the extended optical fiber.

Even though a continuous monitoring of the analyte (substance being measured) can be performed using fluorescent techniques, the measurement is not instantaneous. The response time is limited by the diffusion rate of the analyte into the sensor following a change in analyte concentration.[2] Diffusion follows Fick's

Law and is dependent on the mobility, concentration and the driving force (concentration gradient) of the analyte. The blood gases have a small molecular weight and will diffuse at a fairly rapid rate.

The response time of fluorescent sensors is diffusion rate dependent during transient phases only. At steady state, the measurement is not diffusion rate dependent, but rather is an equilibrium type measurement. Equilibrium reactions are reversible and thus analyte is not consumed in the measurement process. When analyte is consumed, i.e., in membrane selective electrodes currently being used to measure blood gas concentrations, there must be a steady-state diffusion of analyte towards the sensor. In long term applications, the equilibrium measurement is more stable than the diffusion rate dependent measurement.[1]

One of the first sensors involving fluorescent properties was a pH sensor utilizing the dye phenol red.[3] Phenol red was used as an optical absorption indicator. The dye was placed in solutions with different levels of acidity and the pH measured by analyzing the properties of the emission spectrum. Phenol red has two different forms depending on the pH of the solution. Each of these two forms have different optical absorption and fluorescent properties. Therefore, the relative concentrations of the two forms of the dye as well as the fluorescent emissions are determined by the pH of the solution. The measurement of pH is most sensitive when the pH equals the pK_a of the dye.[1] The pK_a of the dye is the point where there is an equal concentration of both the dye states. Changes in the pH around this point will cause large changes between the different forms of the dye. The fluorescent measurement is dependent on relative amounts of the two forms of

the dye. Therefore, when a high degree of sensitivity between dye forms exists, a high degree of sensitivity in the measurment will also be present.

Within the pH sensor, the phenol red was immobilized by bonding to polyacrylamide microspheres (Figure 1). These microspheres were packaged within the pH probe and surrounded by ion permeable cellulose dialysis tubing. The dialysis tubing was attached on one end to the fibers and on the other end to a cap. A green light emitting diode was used to excite the dye, while the red light emitting diode was used to compensate the system. Green light corresponds to the absorption spectral peak of phenol red, and thus provides sufficient energy to excite the dye. Red light has a longer wavelength and lacks the energy to excite the dye. The red light can thus be used to determine the amount of light present at the detector due to reflection and other nonfluorescent optical properities. The green light contains all the characteristics of the red light with an additional intensity which corresponds to the fluorescent signal. The green/red ratio thus provides a signal with compensation for optical variation.

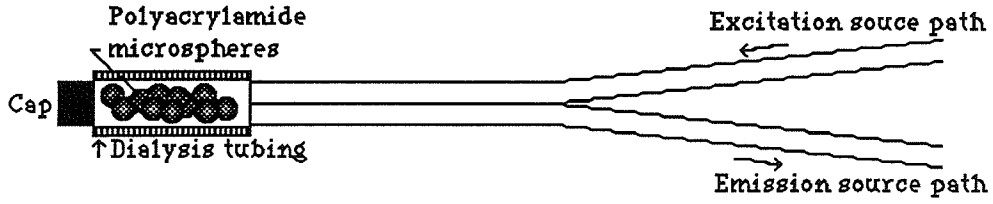

Figure 1 A pH sensor which utilizes the dye phenol red as an optical absorption indicator.

Since the initial design of the pH sensor, numerous other sensors have been developed including a pCO_2 sensor which makes use of a bicarbonate solution in a

gas permeable enclosure.[1] The CO_2 diffuses across the barrier causing a change in the carbonic acid-bicarbonate equilibrium and thus a change in pH at the sensor. The technique described above was then used to measure the pH. The resulting pH measurement was directly proportional to the CO_2 concentration.

A different design of a fiber optic sensor was developed which measures oxygen concentration using photoquenching properties of fluorescent dyes.[1] Aromatic molecules in general absorb light in the ultraviolet and visible regions. This energy can be held in the excited state for a relatively long period of time, i.e., 1 nanosecond. When the fluorescent dye remains in the excited state for long periods of time, there is a greater probability of collisions occurring with other molecules. The energy is then transferred between the molecules and the fluorescence is quenched. This photoquenching effect is linearly related to the collision rate between the dye and the O_2 molecules. In this case the observed mean lifetime of the dye, rather than the intensity, was used to measure the oxygen concentration.

An interesting example of a fluorescent dye involving a reversible measurement technique is a competitive binding sensor. A competitive binding sensor combines the technique of competitive binding assay with fluorescence in a fiber optic device. One such device has recently been developed to measure glucose.[2] In this instrument, there is a fluorescent tagged indicator (FITC dextran) which competes with glucose for binding on a substrate (concanavalin-A). A schematic diagram of the sensor is shown in Figure 2. The indicator in Figure 2 is

labeled "i," the substrate is labeled "s" and the glucose is labeled "g." The optical excitation is coupled to a region of the sensor that contains the indicator alone. The substrate is located such that both the FITC dextran and the glucose must diffuse through barriers before binding to the substrate. A barrier is created using dialysis tubing such that the indicator is free to diffuse into the chamber containing the substrate, but is prevented from diffusing out of the sensor. The glucose is free to pass into the sensor and bind to the substrate. In the absence of glucose a large amount of the indicator is bound to the substrate. Then, as the glucose concentration increases, the glucose will diffuse into the sensor and compete for binding sights on the substrate. The indicator will equilibriate between the chambers and there will be a higher concentration of indicator within the optical excitation chamber. Thus, greater concentrations of glucose will correspond to a larger fluorescent signal. This technique is applicable to many systems which require a competitive binding mechanism to take place.

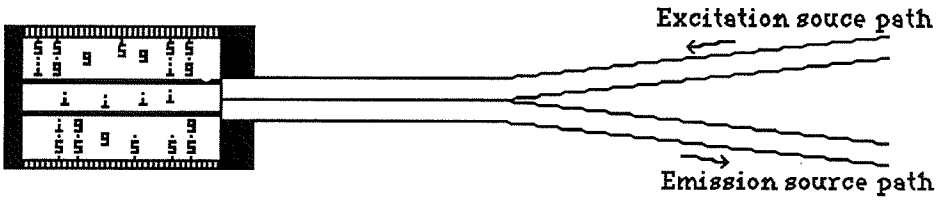

Figure 2 A glucose sensor utilizing a competitive binding technique.

A common technique used to detect the spectral emission of a fluorescent dye is shown in Figure 3. The major function of the light source is to excite the dye at the peak spectral excitation wavelength, or wavelengths, specific for the dye. The

Figure 3 A technique used to detect the spectral emission properties of a fluorescent dye. The fluorescent dye is contained within the sensor.

light source can be either a continuous or a time-varying source, depending on the parameters of the system. A pulsed light source would be best suited to avoid photodegradation of the dye. The advantage of a constant light source is that much of the noise can effectively be eliminated by using a low pass filter. The filter, when placed at a low frequency, prevents the higher frequency noise components from entering the measurements. One problem with continuous sources is that they are less stable than a time-varying source.

The fluorescent dye need not be bound to the end of the optical fiber for sensing to take place. In some applications the dye is free in solution and a bare-ended fiber optic is used to make measurements. There are two common techniques employed when the dye is freely suspended in the solution. The first is shown in Figure 4a. In this case there is a separate fiber for fluorescent excitation and emission. The fiber carrying the fluorescent emission is usually oriented at a 90^{o} angle with respect to the excitation fiber. This angle allows the detection of fluorescent emission with only a small addition due to the excitation light which has been reflected by the solution. The second technique uses one optical fiber for both the excitation source path and for the return path of the spectral emission, Figure 4b.

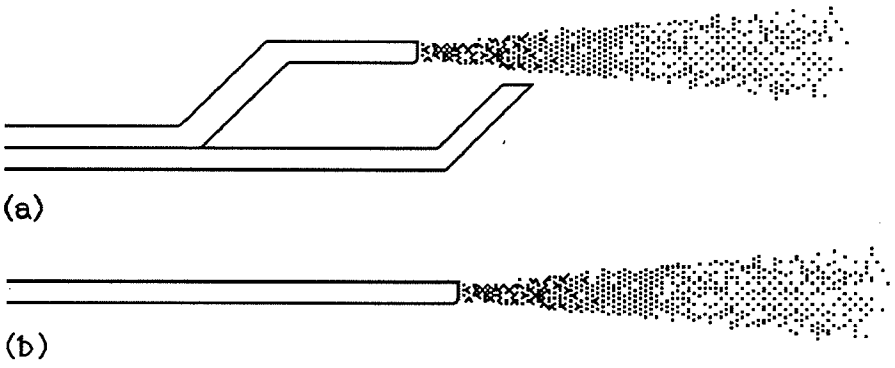

Figure 4 Fiber optic sensors with the fluorescent dye freely suspended in solution. Sensor (a) contains a separate fiber for the excitation source and the fluorescent emission. Sensor (b) utilizes the same optical fiber for both excitation and emission signals.

In most cases the fluorescent dye is not freely suspended in solution, but instead is immobilized at the end of an optical fiber. The immobilization can be accomplished by covalently bonding the dye to the end of the optical fiber. A covalent bond provides the best means of attachment; however, for many dyes the covalent bond alters the spectral properties of the dye. The most common technique of dye immobilization is by providing a barrier to diffusion such that the dye cannot diffuse out of the sensor, but the analyte can diffuse in. The measurement techniques for an immobilized dye are similar to those described above. There can be separate optical fibers for excitation path and the emission path (Figure 5a), or a single optical fiber is used to accommodate both signals, Figure 5b.

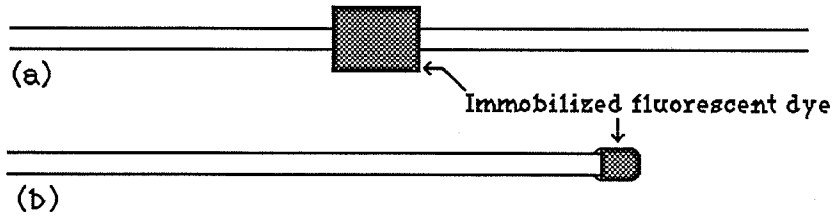

Figure 5 Fluorescent sensors with the fluorescent dye immobilized within the device. Sensor (a) utilizes two fibers, one for excitation of the dye and the other for fluorescent detection of the signal. Sensor (b) utilizes one optical fiber for both excitation and detection.

The detector measures the fluorescent spectral emission following excitation of the dye. If the dye has multiple excitation wavelengths, the peaks can be separated using a set of beam splitters and band-pass filters. Multiple detectors can then be used to measure each spectral emission peak characteristic for the dye. The optical signal is detected and converted to an electrical signal. In many situations the return light flux is weak and the electronics must be optimized to achieve a good signal-to-noise ratio.

The medical need in hyperthermia cancer therapy for a simultaneous pH and temperature measurement brought about the instrument described here. An optical instrument could be used to measure the intratumor pH during microwave-induced local hyperthermia treatment without the problems associated with conventional electrical transducers. Intratumor pH is of considerable interest during hyperthermia treatment. Tumors initially grow at a rapid rate often causing their blood supply to be less structured than that of normal tissue. Thus, when a tumor undergoes hyperthermia treatment the blood supply to that area decreases as opposed to normal tissue which has an increased blood supply under the same conditions. The increased temperature and the decrease in blood flow cause lactic acid to build up within the tumor which in turn causes a decrease

in the intratumor pH. The temperature is also an important factor during hyperthermia treatment. The effectiveness of hyperthermia treatment is currently assessed by mapping the temperature distribution following the treatment.[4] An instrument having the ability to measure both the pH and temperature will allow a continuous measurement of these variables. The results can then be mapped out and compared with the degree of tumor damage. The results could provide insight concerning the effectiveness of different hyperthermia treatment schedules.

CHAPTER 2

STUDIES OF OPTO-ELECTRICAL TRANSDUCTION SCHEMES

There are several different types of optical radiation detectors currently available. The pin photodiodes, used in the design, were chosen on the basis of their performance and versatility. A study of the theory of operation of the pin photodiode and other optoelectric detection devices is presented here. There are advantages and disadvantages associated with each of the devices. The characteristics of these devices differ and so an understanding of their properties is useful in determining the suitability of a device for a specific application. The solid-state detection devices discussed include the pin photodiodes, photomultipliers, avalanche photodiodes and photoconductors.

With sufficient energy applied to a particular material, valence electrons will be released. The energy required to create an electron-hole pair is between 0.2 to 3 eV, corresponding to wavelengths between 6,200 and 413 nm. For an optoelectric device the incident light energy creates an electron-hole pair which alters the current flow through the detector. The similarity that describes all the solid-state photodetectors listed above, is that each device is a square-law detector. In this case the signal photocurrent is proportional to the optical signal power which satisfies square-law conditions.

2.1 Photoconductor

A photoconductor consists of a single layer of photoconductive material. This photoconductive layer has a resistance which decreases upon light illumination.

Light incident on the photoconductor creates electon-hole pairs which alter the current within the device. The signal voltage generated is given by Equation (2-1).[5]

$$S = \frac{V_b \, R_L \, \Delta R_d}{(R_L + R_d)^2} \qquad \textbf{(2-1)}$$

where

V_b = detector bias voltage

R_L = load or feedback resistance in the amplifier circuit

R_d = detector resistance.

An external voltage source is necessary in order to induce electron flow through the detector. These electrons may then recombine with the available holes at the negative photoconductive terminal. A schematic diagram of a bulk photoconductor is shown in Figure 6. In order to maximize the change in resistance with light flux, the material must be relatively transparent to the incoming photons. Transparency refers to the ability of the photon to pass into the device and is a function of the incident wavelength and the photoconductive material. The material should be chosen such that there is as little light reflection as possible. In other words, the energy gap should be less than the energy of the arriving photon. There is a significant fall in the response of the photoconductor at the longer wavelengths due to the photon not having sufficient energy to create an electron-hole pair. At shorter wavelengths the response again falls due to recombination near the detector's surface, where the higher energy photons are more likely to strike.

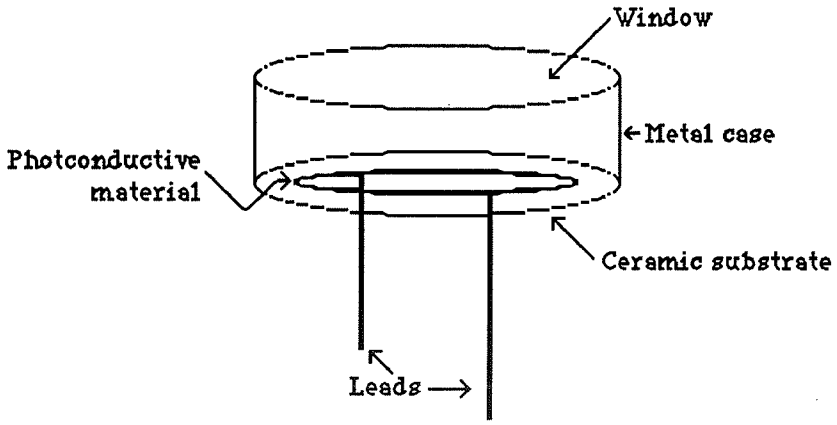

Figure 6 Diagram of a bulk photoconductor.

The large area and the lack of a pn junction allow the photoconductor to have a fairly high sensitivity. In fact, at high light levels the photoconductor gives similar or better sensitivity results than the photodiode.[6] Lacking a junction potential, one would think that the photoconductor would have a large frequency bandwidth. This is a false assumption; the photoconductor tends to have a fairly slow response. The rise time of the photoconductor, following a step input, is fairly rapid. The fall time, however, is slow due to the time required for the electron energy level to return to the valence band. The rate of electron energy loss is related to imperfections within the photoconductive material.

Resistive photoconductors tend to be temperature sensitive. This sensitivity is dependent on the material and the light flux incident on the device. Operation at higher light intensities offers better temperature stability. Photoconductors possess light history characteristics, that is, they conduct differently depending on their previous illumination history. The intensity and duration of light within a set time will alter the conductive properties of the device.

2.2 Photodiode

Whereas the photoconductor has electron-hole pairs generated within any portion of the material, the pn photodiode electron-hole pairs are mainly released within the depletion region. The electrons are then swept across the junction before recombining. This flow of charge is the major source of current within the photodiode. In order to increase the junction width of the photodiode, an intrinsic (i) layer is sometimes added between the p- and the n-doped layers, thus the name pin photodiode. A model of a pin photodiode is given in Figure 7. The p-layer is made very thin so that there will be few electron-hole pairs created in this region. The intrinsic layer is made large enough to maximize the probability that the photons will strike within this region yet thin enough to not sufficiently increase transit time of the charges. The latter would have the effect of reducing the bandwidth of the photodiode.

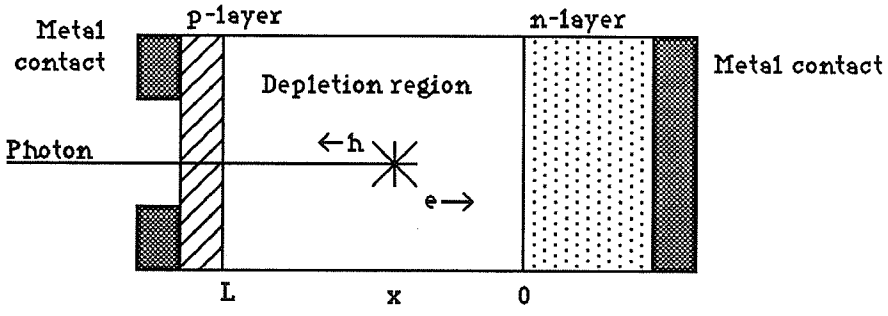

Figure 7 Diagram of a photon absorption within the depletion region of a photodiode. An electron-hole pair is released at point x.

With one photon passing through the p-layer and striking within the depletion layer, two charges will be generated. The electron of charge -q will be attracted to the anode while the hole, of charge +q, will be attracted to the cathode. If recombination takes place within the depletion region, the electron will travel a

distance x and the hole a distance L - x, where L is the width of the depletion region, (see Figure 7). The electron travels at a velocity v_e so the transit time of the electron is given by

$$t_e = \frac{x}{v_e} \tag{2-2}$$

A similar equation for the hole can be derived and the transit time for a hole is given by

$$t_h = \frac{(L - x)}{v_p} \tag{2-3}$$

A current pulse is generated for both the electron and the hole which have the amplitude and duration defined by Equations (2-4) and (2-5) for the electron and Equations (2-6) and (2-7) for the hole.

$$\text{Amplitude} = \frac{\text{Coulombs}}{\text{seconds}} = \frac{e_e}{t_e} \tag{2-4}$$

$$\text{Duration} = \frac{\text{distance}}{\text{velocity}} = \frac{x}{v_e} \tag{2-5}$$

$$\text{Amplitude} = \frac{e_h}{t_h} \tag{2-6}$$

$$\text{Duration} = \frac{(L - x)}{v_h} \tag{2-7}$$

The net charge is determined by the product of the amplitude and duration for each of the charges. The charges are then added together to yield the total charge due to an incident photon, Equation (2-8). Each charge travels only a fraction of the total distance of the depletion layer, and so the current pulse is generated only within this region. The constants k_1 and k_2 account for this reduction of charge and are defined by Equations (2-9) and (2-10) below.

$$\frac{k_1 e_e x}{t_e} v_e + \frac{k_2 e_h (L - x)}{t_h} v_h = k_1 e_e + k_2 e_h \qquad \textbf{(2-8)}$$

$$k_1 = \frac{x}{L} \qquad \textbf{(2-9)}$$

$$k_2 = \frac{(L - x)}{L} \qquad \textbf{(2-10)}$$

Substituting Equations (2-9) and (2-10) into Equation (2-8) the charge due to one electron-hole pair can be calculated, Equation (2-8).

$$\frac{x}{L} e_e + \frac{(L - x)}{L} e_h = e \qquad \textbf{(2-11)}$$

The charge generated for an incident photon, barring recombination, is e. This can be thought of by considering a photon incident directly on the border of the p-doped depletion region. The hole would recombine immediately resulting in no charge. The electron, however, would be swept across the entire length of the

depletion region resulting in a charge e_e. The expression for the signal voltage generated due to incident light flux for a photodiode is given by[5]

$$S = \phi A n e R_L \qquad (2\text{-}12)$$

where

ϕ = incident photon flux

A = detector area

n = quantum efficiency

e = the charge of an electron

R_L = load or feedback resistance in the amplifier circuit.

The photodiode can be operated in either a photovoltaic or photoconductive mode. In the photoconductive mode, a reverse bias is applied causing an increased votage drop across the depletion region. The depletion region is widened by the applied reverse voltage, thus causing the junction capacitance to decrease. This provides an increased bandwidth for the device. This is demonstrated in Figure 8; as the applied voltage is increased, the distance d also increases. Since the capacitance is inversely proportional to the distance between the charge plates; an increase in d will result in a reduction of the capacitance. This assumes that the surface area of the charge plate remains constant, which is true in this case. Although a greater bandwidth can be attained using a reverse bias voltage, there is one disadvantange. A significant increase in dark current occurs when a

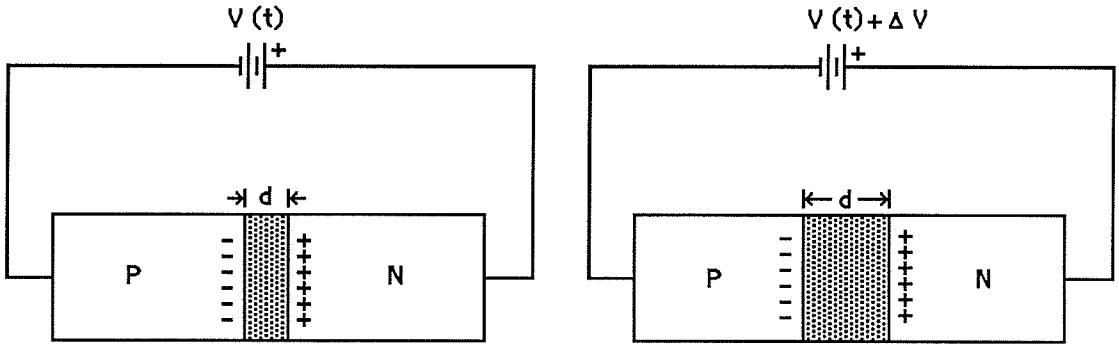

Figure 8 Charge space depletion region of a reversed biased pn junction.

reverse bias voltage is applied. Dark current consists mainly of the thermal emission of electrons at room temperature, but also contains components from leakage current and regenerative effects.[7] The relationships between junction capacitance, dark current and reverse voltage for the Hamamatsu S1722-01 can be seen in Figure 9.[14]

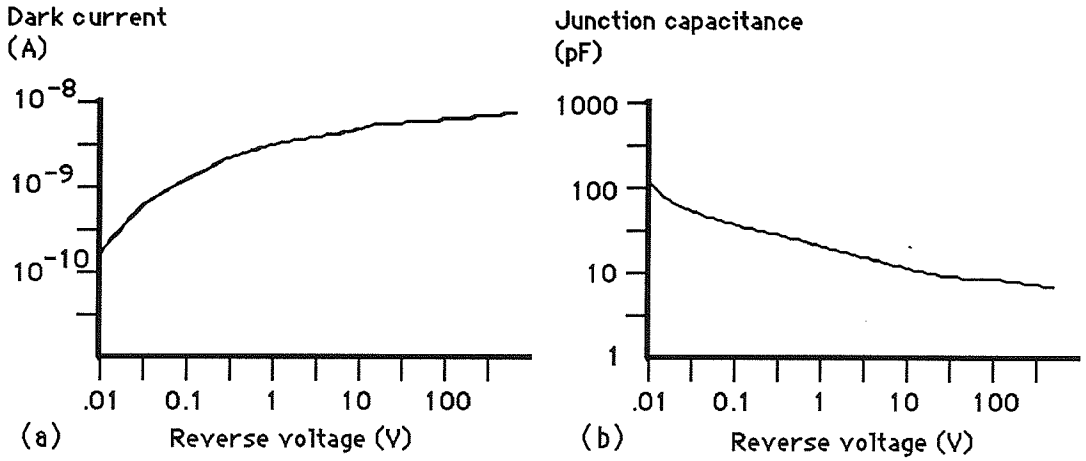

Figure 9 Relationship between the dark current, junction capacitance and the reverse voltage for the Hamamatsu S1722-01 photodiode.

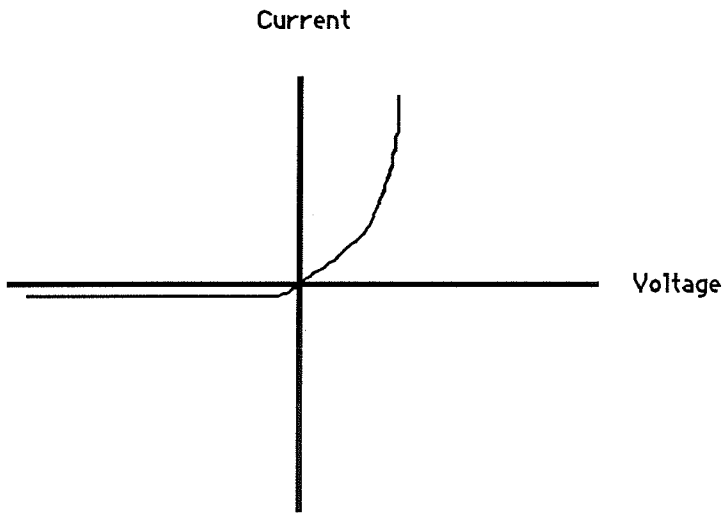

Figure 10 Current/Voltage characteristics for a photodiode with no incident light.

In the photovoltaic mode, there is no bias voltage applied to the photodiode and the incident light flux creates a current as the electron-hole pairs are swept across the junction by the resting junction potential. The current generated by the photodiode will cause its depletion region to be forward biased. A forward biased photodiode has characteristics which are slightly different from a reversed bias photodiode as can be seen in a general voltage versus current plot of a diode, Figure 10. In the photoconductive mode, there is a large voltage change for small changes of current. The inverse of the photoconductive mode occurs in the photovoltaic mode. In the photovoltaic mode, there is a large current change for small changes of voltage. It can be noted that the internal resistance of the photodiode is the reciprocal of the slope of the I-V curve evaluated at a set operating point. A plot of the internal resistance versus the reverse voltage is shown in Figure 11. It follows that a photodiode run in the photovoltaic mode has a smaller shunt resistance. This can be thought of intuitively as the depletion region decreasing with forward bias (Figure 8), thus decreasing the resistance. The

capacitance also is greater for a forward biased p-n junction.

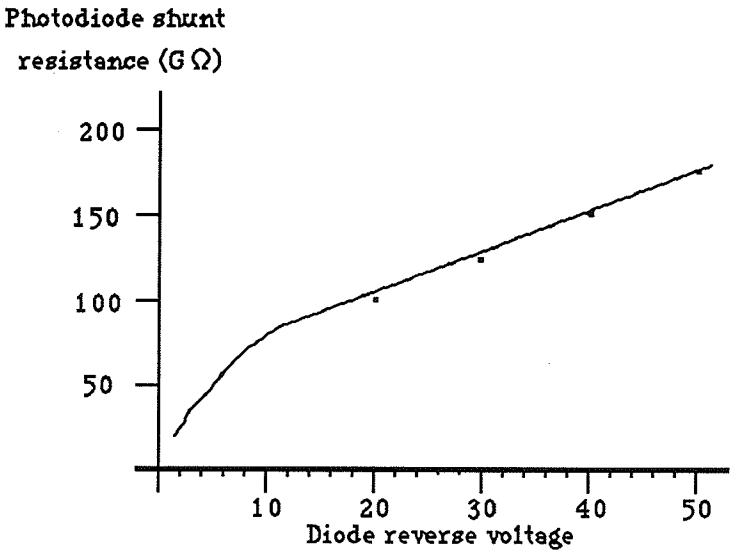

Figure 11 Plot of the photodiode shunt resistance versus the photodiode reverse voltage.

2.3 Photomultiplier Tube

The theory of the photomultiplier tubes involves the photoelectric effect.[7] The external photoeffect involves ejecting electrons from a photocathode in an applied electric field. Incoming photons strike the photocathode causing the release of electrons. The free electrons will be swept away by the applied electric field and will strike a series of dynodes with each successive dynode having a lower potential. The dynodes within the vacuum tube are connected by series resistors as shown in Figure 12. The electrons will be accelerated between the dynodes by the voltage drop across the resistor. As the electron accelerates between the dynodes its kinetic energy will increase according to the equation E=qV. As the excited electron strikes the dynode a number of elecrons will be emitted. With this principle of operation there is a large internal gain in the

device that is dependent on the applied voltage. The signal voltage of the photomultiplier tube in response to an applied light flux can be described by the equation[5]

$$S = \phi A n_k n_d e G R_L \qquad (2\text{-}13)$$

where

ϕ = incident photon flux

A = detector area

n_d = first dynode collection efficiency

n_k = photocathode quantum efficiency at a set wavelength

G = photomultiplier tube current gain

e = the charge of an electron

R_1 = load or feedback resistance in the amplifier circuit

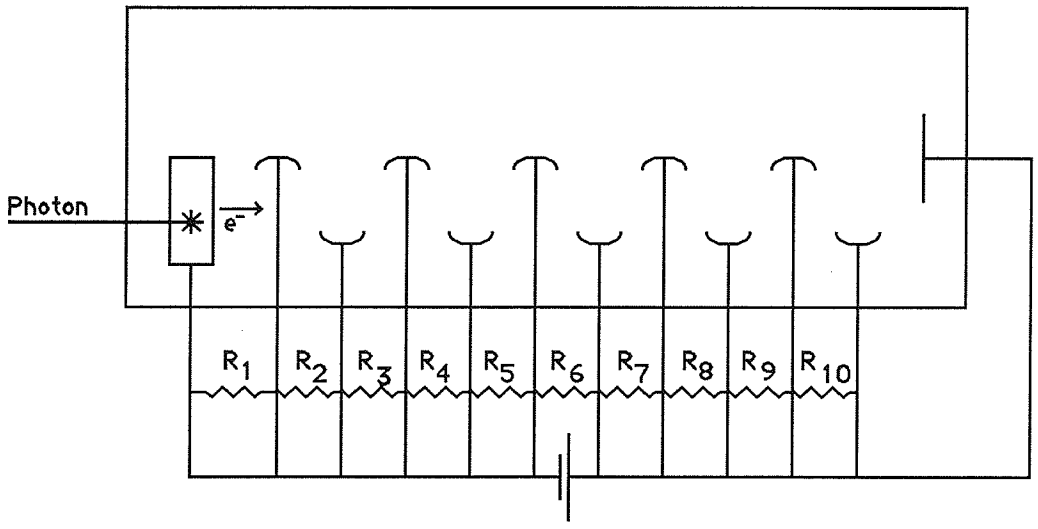

Figure 12 Schematic diagram of a photomultiplier tube.

As is the case for the photodiode, low light intensity measurement is limited by the dark current. The primary source of noise within a photomultiplier tube, however, is the shot noise. Shot noise is defined as the unequal arrival times of photons on the detector. One definite advantage of the photomultiplier tube is the fact that the dynode chain amplification is effectively noiseless.[7] This is due to the fact that the first dynode gain dominates the noise characteristics of the device and the succeeding dynodes produce little in terms of noise. Since there is effectively no amplifier noise, the shot noise of the photocathode, following the same amplification pathway as the signal, is the major noise component. The noise present in a photomultiplier can be described by[8]

$$i_n = \sqrt{M_k [(2eB)(1 + 1/\partial_1 + 1/\partial_1\partial_2 + \ldots + 1/\partial_1\partial_2\partial_3\ldots\partial_k)]} \qquad (2\text{-}14)$$

where

I = the total average photocathode current

$\partial_1, \partial_2, \ldots \partial_k$ = the secondary gains for each of the dynode stages

$M_k = (\partial_1 \partial_2 \partial_3 \ldots \partial_k)$ The total gain of the amplifier

B = the bandwidth

e = the charge on an electron (1.6×10^{-19}).

2.4 Avalanche Photodiode

The avalanche photodiode contains a pn junction to which a large reverse bias is applied. The bias is applied such that the junction voltage is very close to the reverse voltage breakdown of the device. When a photon strikes the junction releasing an electron-hole pair, the electron, and the hole, are accelerated across

the depletion layer. Enough kinetic energy can be gained by the accelerating electron to cause new electron-hole pairs to be released from the valence to the conduction band via impact ionization. The result is a large increase in junction current. The large electric field creates a situation similar to the photomultiplier in which current multiplication takes place.

Avalanche photodiodes are similar in their construction to normal pn photodiodes, with the exception being the special care taken to assure uniform junction fabrication. An equivalent circuit for the avalanche photodiode appears very much like that of the pin photodiode with the addition of a current multiplication factor M, seen in Figure 13. The avalanche photodiode offers

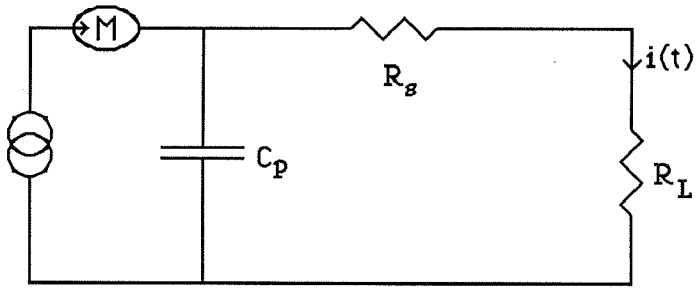

Figure 13 Equivalent circuit model for an avalanche photodiode.

features similar to those of the photomultiplier yet it is more compact and has a lower bias voltage. The noise characteristics, however, favor the photomultiplier which has a fifth of the dark current noise of the avalanche photodiode. The noise current within an avalanche photodiode can be described by the equation[8]

$$i_n = M^2\sqrt{(2eIBM)} \qquad (2\text{-}15)$$

where

I = the total average current before multiplication

M = the multiplication factor

B = the bandwidth

e = the charge on an electron (1.6×10^{-19}).

2.5 Discussion

The optical signal returned from the fluorescent dye of a fiber optic sensor is quite low, on the order of nanowatts. With this in mind, the photoconductor will probably not have the sensitivity required to accurately measure the return signal. Advances in photoconductor technology have resulted in high speed photoconductors with excellent temperature stability. Nevertheless, photoconductors tend to be used mainly in high light intensity applications where their advantages are low cost and high sensitivity due to their large surface area.[6] Avalanche photodiodes are generally noisy due to the multiplication factor M (Equation (2-15)) which increases the noise over the noise-free amplification by a factor of $M^{1/2}$.

The photomultiplier tube, having a high sensitivity in the ultraviolet/blue spectrum and essentially noise-free gain, is well qualified for this application. However, there are disadvantages associated with the photomultiplier. It requires more external circuitry including a high voltage power supply. The photomultiplier dark current is generally larger than that of the photodiode. This is generally compensated for by the noiseless gain of the photomultiplier versus the noise induced during amplification of the signal from the photodiode.

Photomultipliers also tend to be bigger and more expensive than the other optoelectric detectors. The pin photodiode is simpler to use, is less expensive and does not require a large voltage supply. With careful circuit layout, low noise amplifiers, and noise optimization techniques, it was felt that sufficient sensitivity could be attained using the pin photodiode.

CHAPTER 3

METHODS

3.1 System

A block diagram of an optoelectrical system that could be used to measure tumor pH and temperature is shown in Figure 14. The fluorescent dye to be used is 1,4-dihydroxyphthallonitrile (1,4-DHPN) shown in Figure 15. This dye has spectral emission properties which are pH dependent. The advantage of using 1,4-DHPN is that it requires a single broadband excitation in order to excite both the acid and base forms of the dye. Many fluorescent dyes require a dual-excitation source because their emission spectra are dependent on both the intensity and the wavelength of excitation. Single source excitation with multiple emission allows a ratio technique to be used to detect the return light flux. There is a high degree of stability when the ratio technique is used because each of the emission wavelengths is exposed to the same optical system. Therefore, fluctuations within the optical system are virtually eliminated.

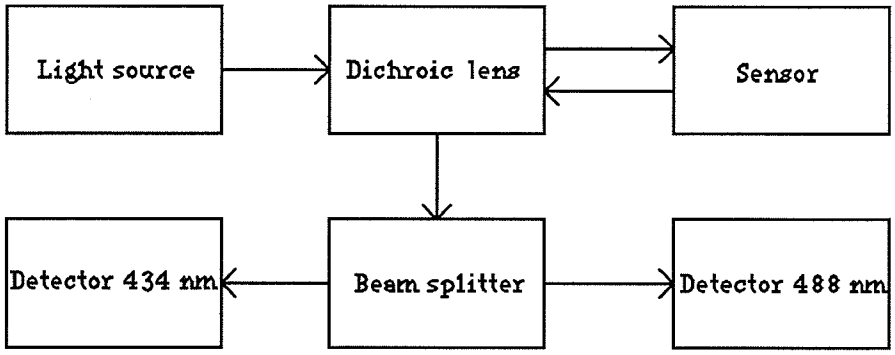

Figure 14 Block diagram of the optoelectric system used to measure tumor pH.

The development of an optical pH and temperature measurement instrument requires both optical and electronic supporting instrumentation. A light source is necessary to excite the dye. The light source is chosen such that there is an optimal transfer of energy within the optical excitation bandwidth of the dye. The optical energy must then be transferred to the sensor with minimal losses and the fluorescent signal detected. A Xenon flashlamp is used as the broad-band excitation source. It is operated at a low frequency, between 8 and 40 Hz, and can produce between 5 to 0.5 joules of energy per flash, respectively. Since the flash duration is on the order of microseconds, the power generated by the flashlamp is quite large. This energy is coupled to the sensor through the input optical fiber of the sensor module.

(a)

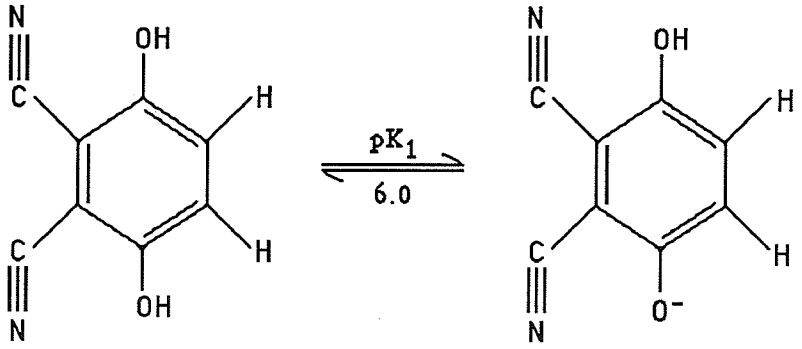

(b)

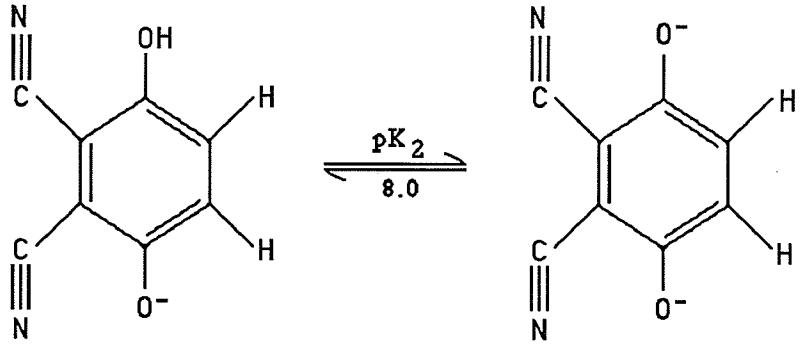

Figure 15 Conversion of the dye 1,4-dihydoxypthallonitirile between the acid and neutral form (a) and the neutral and basic form (b).

Detection of the optical signal at each emission peak is accomplished by a pair of pin photodiodes. The photodiodes generate a current that is proportional to the incident light signal. The current is converted to a voltage by means of an operational amplifier connected in a current-to-voltage configuration. The signal is further processed using an integration technique which integrates the signal for a short period of time following the discharge of the flashlamp. A variable gain amplifier is then used to amplify the signal before it is passed to an analog-to-digital converter within the Apple 2e computer. Once digitized, the ratio of the signals is calculated using a software program, and the pH determined.

3.2 Sensor

The fluorescent dye 1,4-dihydroxyphthallonitrile (1,4-DHPN), shown in Figure 15, has been shown to be pH sensitive within physiological ranges (nominal pH of 7.4).[9] It can also be seen from Figure 15 that the dye has different ionization forms depending on the hydrogen ion concentration of the solution. The pK_a's of the dye are 6.0 for the acid form and 8.0 for the basic form. Both forms of the dye have fluorescent properties and emit light following excitation from a single broad-band source. The excitation spectra for the acid and the base forms are shown in Figure 16. The peak excitation wavelength is found at 387 nm. Following excitation the spectral emission characteristics have peak wavelengths of 434 and 488 nm corresponding to the acid and base forms, respectively. In Figure 17 the fluorescent light intensity is plotted as a function of wavelength at pH 6.0 and 8.0. This figure displays the peak emission characteristics for the two forms of the dye. As the pH of a solution changes, within the physiological ranges, the light intensities at the two emission wavelengths should change inversely with one another. Thus the ratio of light intensities at the peak emission wavelengths contains information pertaining to the pH of the solution.

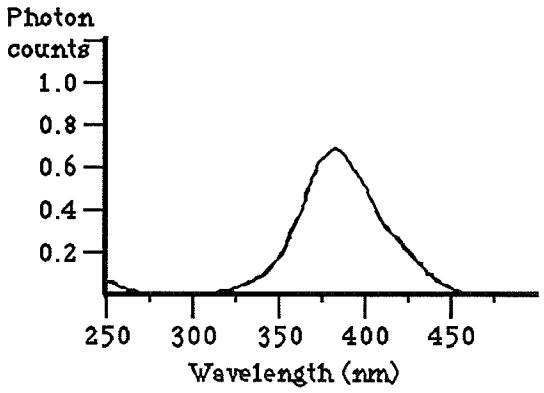

Figure 16 Excitation spectral peak for 1,4-DHPN.

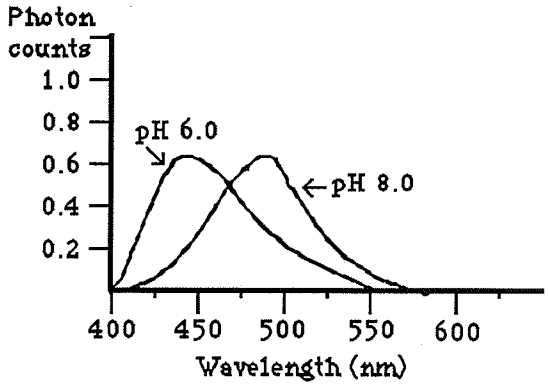

Figure 17 Spectral emission peaks for 1,4-DHPN at pH 6.0 and pH 8.0.

3.3 Optics

The design of the optical system is based on the physical properties of the dye. Considering that 1,4-DHPN has dual fluorescent emission characteristics following a single excitation, a single light source will be sufficient. A Xenon flashlamp is used for the light source with the optical energy being transferred to an optical fiber via a parabolic mirror and two convex lenses. The optical fibers are made from a special silica which can effectively transmit wavelengths below 400nm. The optical energy produced by a Xenon flashlamp is broadband and a

bandpass filter is used to limit the energy to wavelengths between 300 and 400 nm. Since the peak excitation of the dye is at 387 nm, only a fraction of the available energy of the flashlamp is used for excitation.

The optical energy is transferred from the flashlamp via an optical fiber to the first optical module. Within this module the light encounters a dichroic mirror at a 45-degree angle. The wavelengths above 400 nm are passed through the dichroic mirror while those below 400 are reflected. The mirror is oriented such that the incoming energy, with wavelengths (λ) between 300 and 400 nm, is reflected to the sensor. The dye is excited and the fluorescent signal ($\lambda > 400$ nm) returns within the same optical fiber to the dichroic mirror where it is passes directly to the output of the module. The output of the first optical module is connected to the the input of the second optical modules by a fiber optic link. The second optical module contains a 45 degree beam splitter and bandpass filters to isolate the two fluorescent signals. The bandpass filters have a center frequency of 434 and 488 nm with a passband of 10 nm.

The optical signals at 488 and 434 nm are finally transferred using optical fibers from the second optical module to pin photodiodes located in the electrical subsystem. A schematic diagram of the optical system is shown in Figure 18. A diagram displaying the internal construction of the two optical modules is shown in Figure 19. The wavelengths corresponding to $\lambda<400$ nm are the excitatory wavelengths while the wavelengths greater than 400 nm correspond to the photoemission of the fluorescent dye.

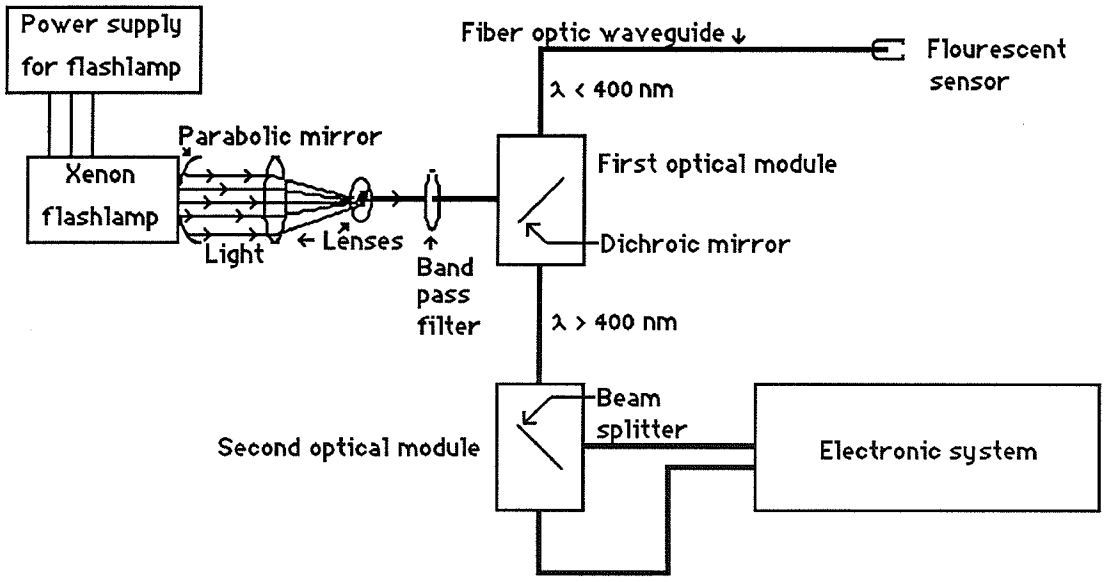

Figure 18 Schematic diagram of the optical subsystem.

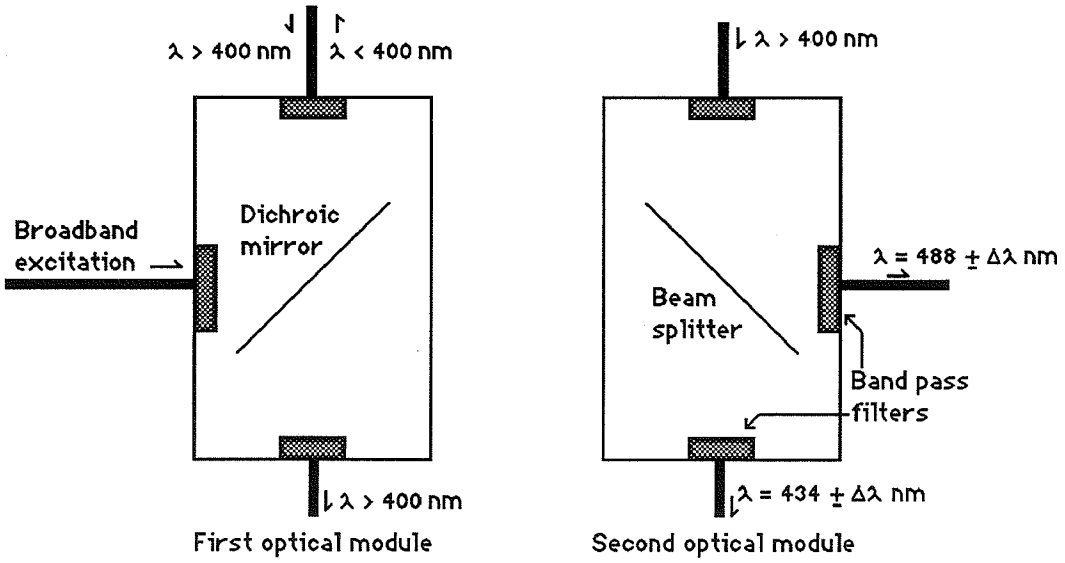

Figure 19 Schematic diagram of the optical modules.

There are many factors that contribute to losses within the optical system. The Xenon flashlamp has the potential of producing large amounts of power, but

only a fraction of this is utilized due to the limited excitation spectrum of the dye. At the sensor, the fluorescent energy is emitted in all directions with only a fraction of this energy returned to the optical fiber. There is a 50 dB loss of optical energy at the sensor. In addition, there is a 1.5 dB loss of energy at each fiber optic connection and there are seven connectors per channel amounting to a total energy loss of 10.5 dB. There is also a loss of energy due to the beam splitter (3 dB) and the bandpass filters (1.2 dB). These losses are cumulative and result in a very low light signal at the pin photodiodes. Thus the detection of these low level light fluxes is crucial to the effective operation of the entire system.

3.4 Electronics

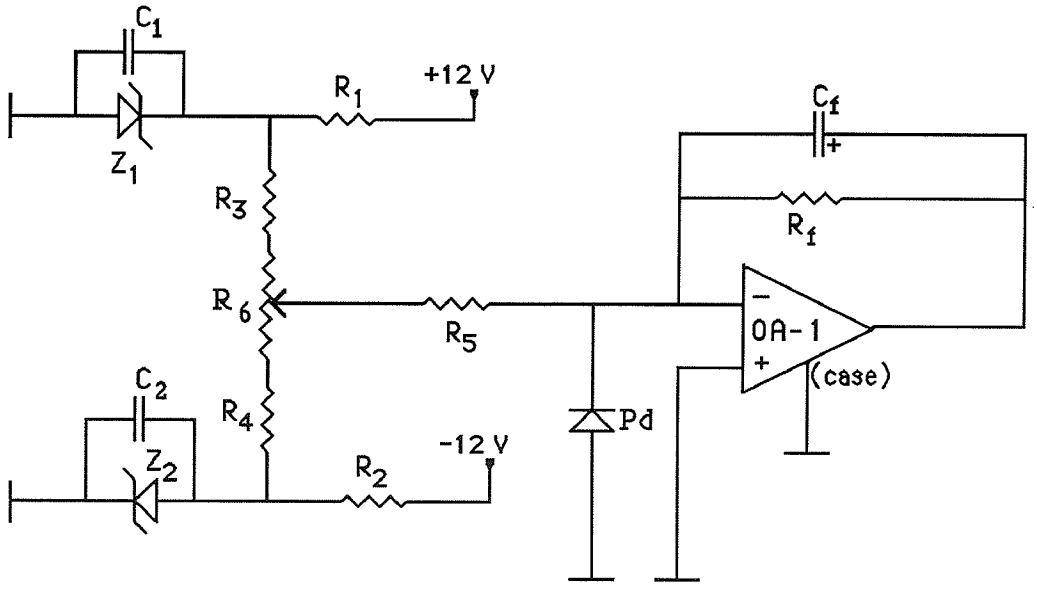

Figure 20 Circuit diagram of the analog front end.

The conversion of the optical energy to an electrical signal takes place within the analog front end. The analog front end consists of a pin photodiode-operational amplifier pair connected in a current-to-voltage converter

configuration, Figure 20. The sensitivity of the front end is extremely critical for measuring low light intensities and achieving a significant signal-to-noise ratio. The pin photodiode sensitivity is shown in Figure 21. There is a linear relationship between the incident light power and the current generated. Since the signal is on the order of nanowatts, the photodiode current will be on the order of nanoamps. Considering the low current signal, special care must be taken to prevent environmental noise pickup. The Xenon flashlamp produced a large amount of radio frequency noise. This noise was greatly reduced following shielding of both the photodiode and the operational amplifier and the connections linking the two devices.

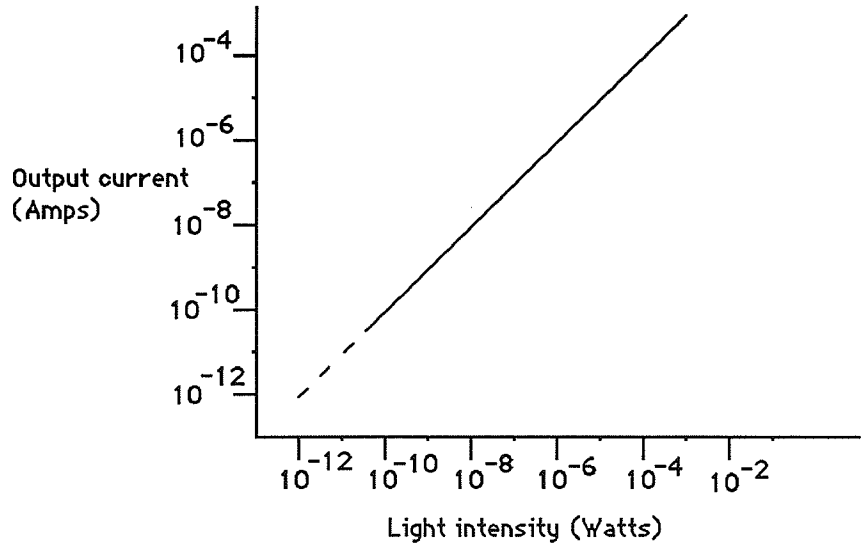

Figure 21 Hamamatsu S1722-01 photodiode senstitivity data.

A current generated within the photodiode of Figure 20 would be seen as a voltage drop across the feedback resistor R_f. Simple analysis, assuming an ideal

operational amplifier, reveals that the output voltage is related to the input current by the expression

$$V_{out} = - R_f I_{in} \qquad (3\text{-}1)$$

The feedback resistor is generally quite large, on the order of 10^7 to 10^9 Ω, in order to measure the weak light fluxes. A large transconductance gain ($V_{out}/I_{in}= -R_f$) associated with a large feedback resistor, will create a situation in which small amounts of noise current induced on the leads between the photodiode and the operational amplifier would produce a significant voltage noise at the output. In addition small dc currents such as the input bias current of the operational amplifier would also be amplified. In order to compensate for the small dc currents, which would manifest themselves as an output voltage offset, a current injection circuit is added to the inverting terminal of the operational amplifier, seen in Figure 20. The zener diodes give a stable voltage reference and set a stable current through the series network R_3, R_4 and R_6. Small changes in the potentiometer R_6 will alter the voltage across R_5. Considering that the inverting terminal of the operational amplifier is at a virtual ground the output voltage due to the effects of the current injection circuit is given by

$$V_{out} = \frac{R_f [V_{z2}(R_T - x + R_2) - V_{z1}(R_1 + x)]}{(R_1 + x)(R_T - x + R_2) + R_3R_1 + R_3x + R_3R_T - R_3x + R_2R_3} \qquad (3\text{-}2)$$

The variable x has the range of [0,1] and is used to describe the position of the potentiometer. If the potentiometer is set such that it divides R_6 exactly by 2, then x=0.5.

The flashlamp operates at a single frequency which can be varied between 8 and 40 Hz. The fluorescent signal associated with each flash is a short exponentially decaying pulse with a time constant in the order of several nanoseconds. The second stage in the processing of the electrical signal is an integration of this signal for a short duration. The integration time should be long enough to detect the complete signal and short enough to reduce the effects of output offset voltages. The sensitivity is also increased by integrating only when the signal is present. The integrator, shown in Figure 22, assists in limiting the noise due to the fact that the signal will add over time while the noise increases by the square root of the noise. This would argue for a longer integration time to increase the signal-to-noise ratio. The actual integration time is 25 μsec.

Each integrated sample is further amplified by means of a variable gain amplifier before passing to a sample and hold device. The gain of the variable gain amplifier can be set at 1, 10, 100 or 1000 depending on the amplitude of the signal. The sample and hold will maintain a steady voltage before the dc signal is converted to a digital signal by an analog-to-digital converter within the Apple 2e computer. Control to the integrator, variable gain amplifier and the sample and hold is all done by the Apple 2e. A complete circuit diagram for one channel of the electrical system is given in Appendix A.

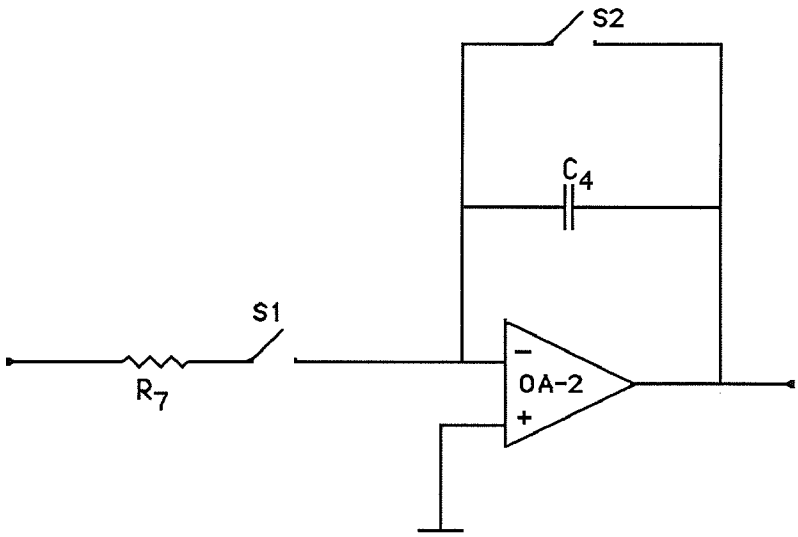

Figure 22 The integrator circuit which follows the current to voltage conversion.

CHAPTER 4

FREQUENCY DOMAIN ANALYSIS

The analysis of the electrical properties of the detection and amplification schemes can offer valuable insight into the optimal design of the front end system. Before offering optimization methods, the constraints of the system are discussed and the optimal design determined accordingly. A design is implemented to maximize the signal-to-noise ratio and to preserve the shape of the fluorescent signal as much as possible.

4.1 Photodiode Characteristics

The two major properties of a photodiode which limit its frequency response are the drift time of carriers across the depletion region and the junction capacitance of the device.[10] The carrier drift time is defined as the finite time required for an electron to be swept across the depletion layer. The bandwidth limited by the carrier transit time is variable but is generally on the order of 10 GHz and is not considered a factor in the present analysis. The junction capacitance (C_p), however, can limit the frequency response of the photodiode. The equivalent circuit model for a photodiode is shown in Figure 23. Note that the pole of the circuit is described by the equation

$$f_{3db} = \frac{1}{2\pi C_p R_t} \qquad (4\text{-}1)$$

where C_p is the juction capacitance and R_T is the equivalent resistance given as

$$R_T = \frac{R_p (R_L + R_S)}{(R_p + (R_L + R_S))} \qquad (4\text{-}2)$$

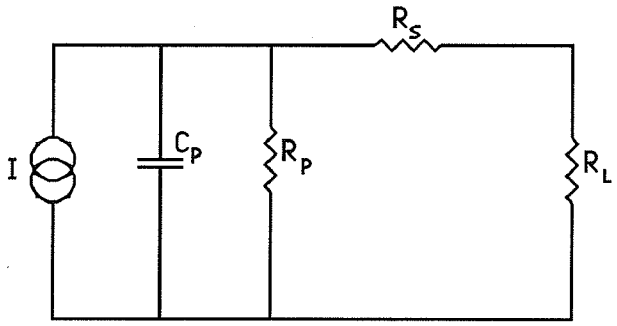

Figure 23 Equivalent circuit model for a photodiode.

Since the junction capacitance is dependent on the reverse bias of the photodiode, shown in Figure 9, increasing the reverse bias voltage applied to the photodiode will decrease the capacitance and increase the frequency response of the device.

The load resistor can also limit the frequency response of the photodiode. The limitation occurs when the shunt resistance of the photodiode is much larger than the load resistor. When this condition holds, the effective resistance of the two resistors in parallel is closer in magnitude to the load resistance. The parallel combination of these two resistors (Equation (4-2)) plays a significant role in determining the frequency response of the photodiode, Equation (4-1). With an applied reverse voltage across the photodiode, the shunt resistance of the device is on the order of $10^9\ \Omega$. Therefore, the main contribution to the equivalent resistance is the load resistor. In the photovoltaic mode, the shunt resistance drops considerably and it may influence the equivalent resistance.

The internal resistance of the photodiode is dependent on the bias applied to the photodiode. The larger the depletion region the greater the internal resistance of the device, as was shown in Figure 8. This can be seen from the current-voltage characteristics of the Hamamatsu S1722-01 photodiode. As was discussed earlier, the internal resistance of the device can be determined from the reciprocal slope of the I-V curve. This curve was discussed in Chapter 2 and can be seen in Figure 11. The junction capacitance and the internal resistance of the photodiode can then be used in the frequency analysis of the photodiode.

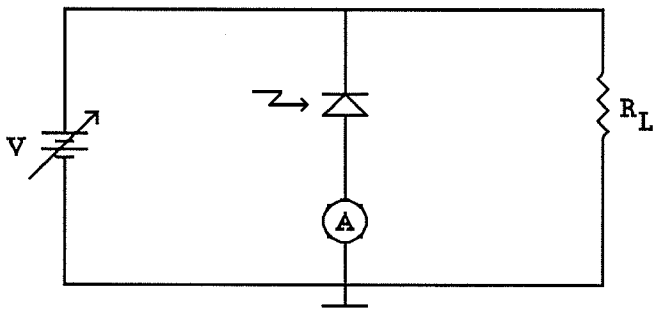

Figure 24 Circuit used to measure the reverse saturation current of the photodiode.

In order to minimize the dark current, the photodiode voltage is clamped to zero using the virtual ground characteristics of an inverting operational amplifier. The internal resistance of the photodiode is measured using the circuit of Figure 24. The reverse voltage across the photodiode is varied and the current through the photodiode is measured. The resulting current-voltage characteristics can be determined; these are plotted in Figure 25 and should resemble Figure 10. As the voltage increases, the current saturates at what is known as the reverse bias saturation current (I_s); for this device it was found to be 0.3 nA.

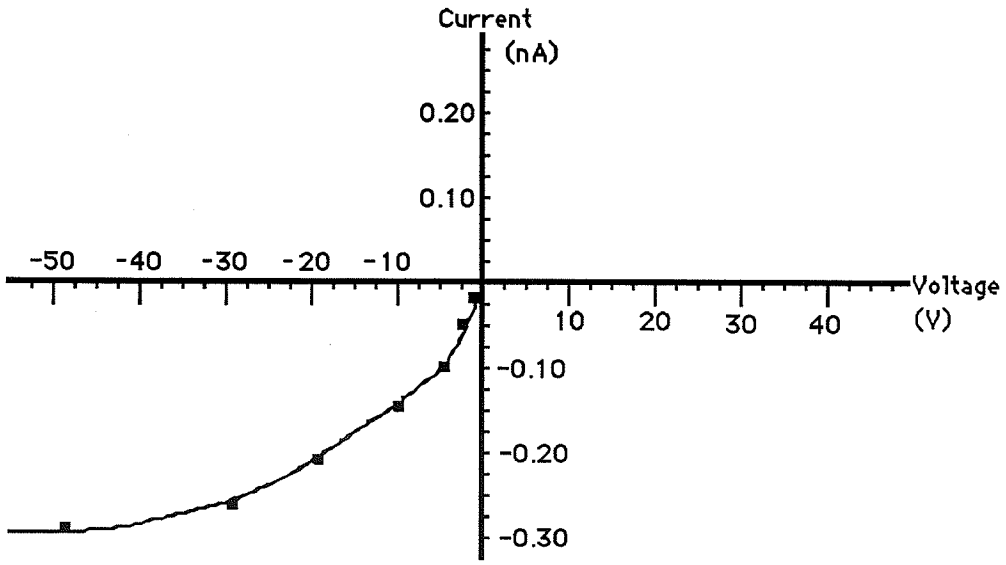

Figure 25 Experimental results of the photodiode current with an applied reverse voltage.

The internal resistance can be calculated at zero bias by using the diode equation. The diode equation is

$$I_d = I_s \left(e^{(qV/kT)} - 1 \right) \tag{4-3}$$

Since the operation point is around zero volts, the exponential term can be described by the Taylor's series expansion given by

$$e^{(qV/kT)} = 1 + (qV/kT) + (qV/kT)^2/\,2! + (qV/kT)^3/\,3! + \cdots \tag{4-4}$$

Substituting this equation into the diode equation and solving for the internal resistance of the photodiode, defined by V/I_d, yields

$$R_p = \frac{V}{I_d} = \frac{kT}{I_s q} \tag{4-5}$$

where

k = Boltzman's constant (1.38×10^{-23})

T = Temperature (300 ^{o}K)

q = Charge on an electron (1.6×10^{-19}).

Substituting these values and the reverse voltage saturation current (I_s) into the above equation determines the internal resistance of the photodiode at zero bias. The result is

$$R_p = 86.25\ M\Omega$$

The internal capacitance of the photodiode was obtained from the Hamamatsu data describing the S1722-01 pin photodiode. The value given was

$$C_p = 100\ pF$$

Using these two values in the determination of the frequency response of the device determines the three-dB down point to be at 18.45 Hz.

Three methods may be employed to increase the frequency response of the photodiode. The first technique is to reduce the load resistor. Reducing the load resistor will lower the equivalent resistance defined by Equation (4-2) and will shift the pole to the left. In other words the 3-dB point will be at a higher frequency. The disadvantage with this is that the noise increases as the square

root of the bandwidth. This will have an overall effect of increasing the noise of the system and of reducing the signal-to-noise ratio of the device. The second method of increasing the frequency response is to apply a reverse bias to the photodiode. This technique causes an increase in shot noise in addition to the noise associated with a greater system bandwidth. The effects of increasing the bandwidth are manifested in an increase of overall system noise. Precautions were taken to minimize the noise while attempting to preserve the signal as much as possible. The third technique is to operate the photodiode in conjunction with an operational amplifier. In this case, not only is the frequency response of the photodiode increased but, as will be shown presently, the signal is also amplified.

4.2 Operational Amplifier Characteristics

In order to effectively convert the photodiode current into a voltage, an operational amplifier is utilized as shown in Figure 26. The photodiode model attached to the inverting terminal of an operational amplifier appears in Figure 26. The operational amplifier used is the Burr Brown OPA101AM, which has open-loop frequency characteristics displayed in Figure 27. Using the open-loop gain and the cutoff frequency of Figure 27, a transfer function can be derived for the operational amplifier. This is done for the inverting model shown in Figure 28. The closed-loop transfer function is given by[11]

$$\frac{V_{out}}{V_{in}} = \frac{-A_o}{[1+(Z_p/Z_f)(1+A_o)+(1+Z_p/Z_f)\,s/w_o]} \qquad (4\text{-}6)$$

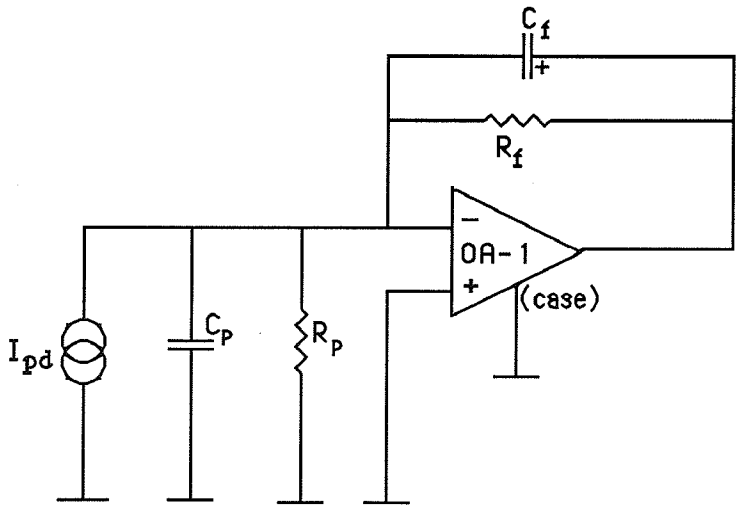

Figure 26 Transconductance gain amplifier with the circuit model for the phototdiode attached.

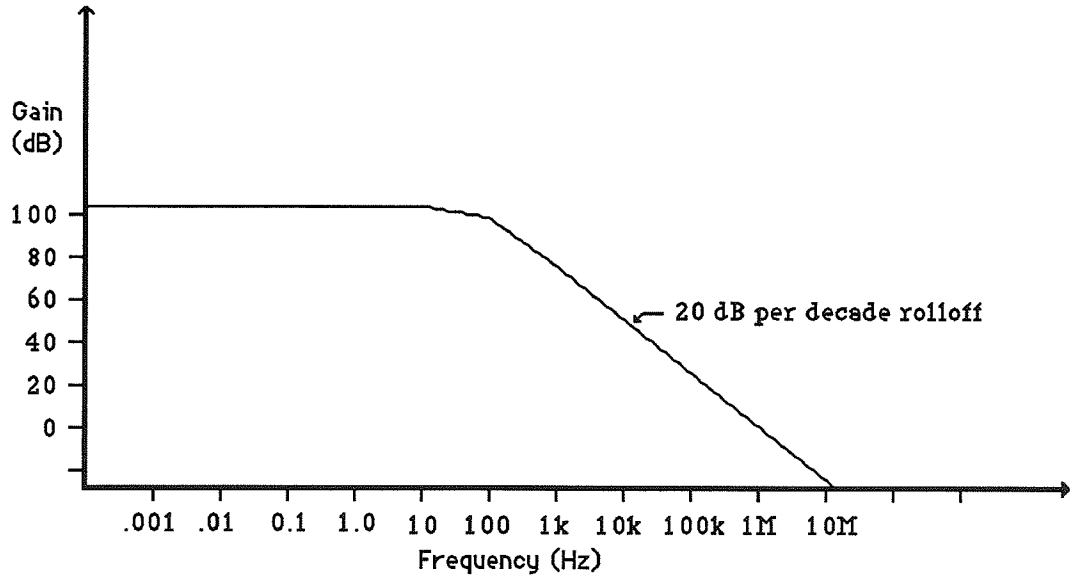

Figure 27 Open-loop gain of the OPA101AM operational amplifier.

The open-loop gain of the OPA101AM is much greater than 1 which simplifies the equation by assuming that $(1+A_0) \sim A_0$. The impedences Z_p and Z_f, shown in Figure 28, are considered to be a resistor/capacitor parallel combination. Using Laplace techniques the combinations are described by

$$Z_p = \frac{R_p}{(1 + s R_p C_p)} \qquad (4\text{-}7)$$

$$Z_f = \frac{R_f}{(1 + s R_f C_f)} \qquad (4\text{-}8)$$

The conversion of the voltage gain amplifier (Figure 28) to a transconductance amplifier (Figure 26) involves changing the voltage source of Figure 28 to a current source using the simple equation

$$V_{in} = - (I_{in}) (Z_1) \qquad (4\text{-}9)$$

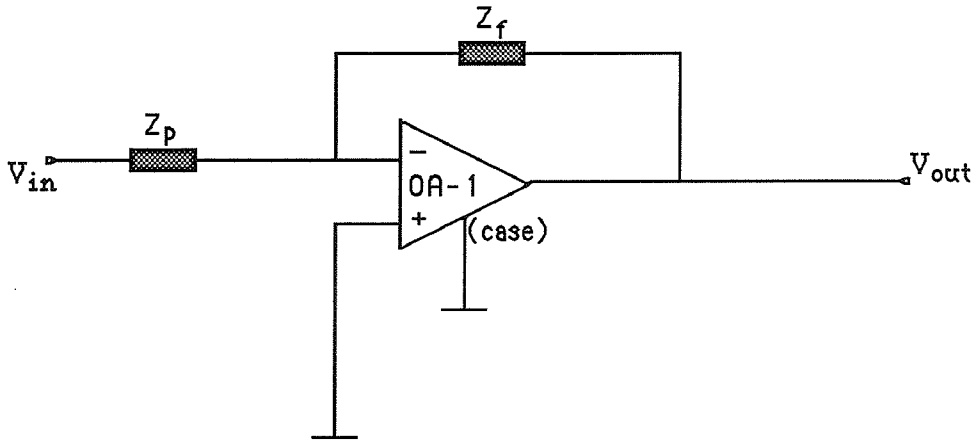

Figure 28 Inverting operational amplifier configuration.

The transconductance transfer function is described by the output voltage devided by the input current. By substituting Equations (4-9), (4-7) and (4-8) into Equation (4-6) the transconductance gain (V_{out}/I_{in}) can be determined. The simplified result is shown in Equation (4-11).

$$\frac{V_{out}}{I_{in}} = \frac{-A_o w_o R_p R_f}{\xi s^2 + \lambda s + \delta} \qquad \textbf{(4-10)}$$

where

$$\xi = R_p R_f C_p + R_p R_f C_f$$

$$\lambda = w_o R_p R_f C_p + A_o w_o R_p R_f C_f + R_f + R_p$$

$$\delta = w_o R_f + A_o w_o R_p \, .$$

Equation (4-10) describes the closed-loop frequency response of the transconductance amplifier shown in Figure 26. It can be seen that there are two poles in the denominator. The magnitude and phase can be determined by replacing the Laplace operator s with jw. The equation can then be simplified and separated into real and imaginary components. The magnitude and phase are calculated according to the equations

$$M(w) = \text{sqr} \, [\, (\text{real})^2 \, \text{x} \, (\text{imaginary})^2 \,] \qquad \textbf{(4-11)}$$

$$\phi(w) = \tan^{-1} [\text{imaginary} / \text{real} \,] \qquad \textbf{(4-12)}$$

The magnitude and phase are

$$M(w) = \frac{w_o A_o R_p R_f}{(\alpha 2 + \beta 2)} \qquad (4\text{-}13)$$

$$\Phi(w) = \tan^{-1} \frac{\beta}{\alpha} \qquad (4\text{-}14)$$

where

$$a = w_o R_f + w_o A_o R_p - w^2 R_f R_p C_p - w^2 R_p R_f C_f$$

$$b = w w_o R_f R_p C_p + w w_o A_o R_p R_f C_f + w R_f + w R_p$$

respectively.

A Bode diagram can be calculated and plotted for the magnitude of the transconductance amplifier defined by Equation (4-14). A 10 MΩ feedback resistor is chosen which sets the gain to be $1x10^7$. This will allow a 0.1 uW light signal, which corresponds to a 0.1 uA current (Figure 21), to be displayed as a 1-volt output signal. The feedback capacitor value is chosen by assuming that stray capacitance is generally between 0.5 and 2 pF. Therefore, if no feedback capacitor is placed in the experimental circuit, a stray capacitance value of 1 pF is used for the default value. The theoretical results of the frequency response calculation are plotted along with the experimental results, Figure 29. Note the significant increase in the frequency response of the device when an operational amplifier is used. The load resistor seen by the photodiode has not changed and yet the frequency response is increased from approximately 20 to 20,000 Hz. When a different feedback capacitor is used the frequency response of the

transconductance gain is altered. As a larger feedback capacitor is used the frequency response of the device drops considerably. Figures 30 and 31 show the theoretical and experimental results for a 51 pF and a 1000 pF feedback capacitor, respectively.

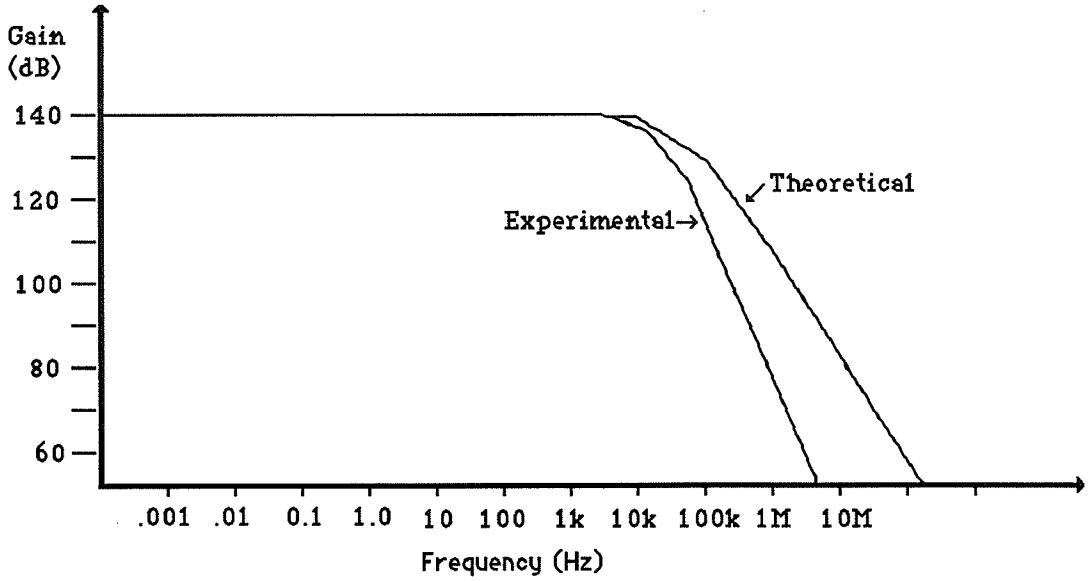

Figure 29 Transconductance gain of the operational amplifier-photodiode circuit with no feedback capacitor.

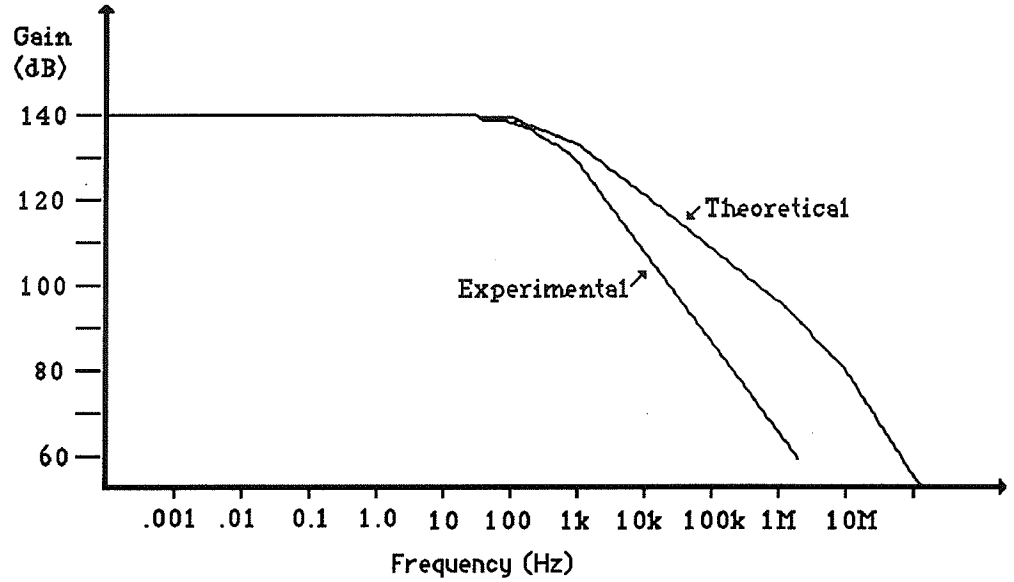

Figure 30 Transconductance gain of the operational amplifier-photodiode circuit with a 51 pF feedback capacitor.

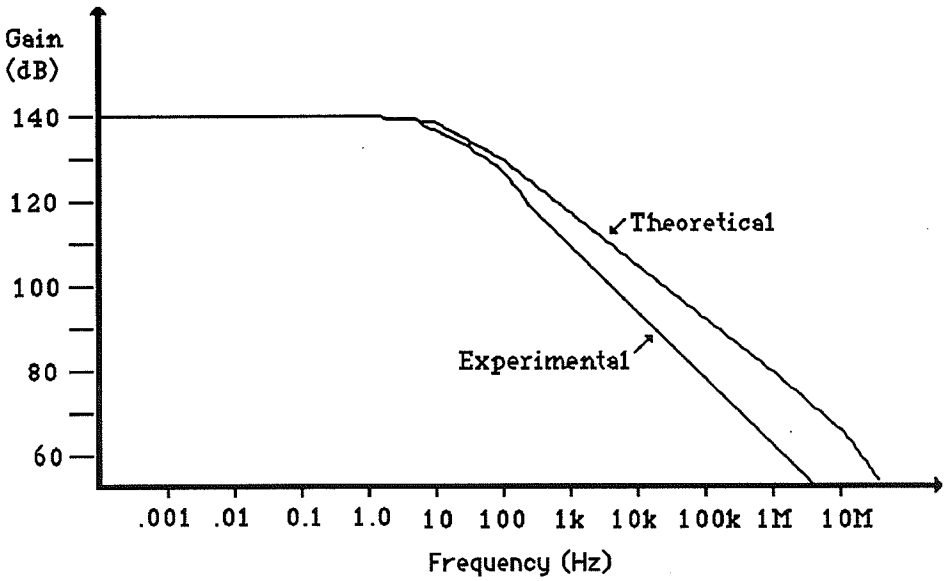

Figure 32 Transconductance gain of the operational amplifier-photodiode circuit with a 1000 pF feedback capacitor.

The frequency response can also be altered by changes in the feedback resistance. The feedback resistance also determines the transconductance gain of the device. Thus a plot can be generated which describes the frequency response as a function of the gain and the feedback capacitor. Figure B-1 (Appendix B) is a contour plot of the frequency response generated on a Cray XMP supercomputer. The feedback resistance, or gain, is along the horizontal axis and is bounded at the lower end by $1x10^5$. The resistor is incremented each hashmark by a multiplication factor of 1.1 until reaching the upper bound at 204 MΩ. The vertical axis describes the feedback capacitance and is bounded by 1000 pF at the origin. The feedback capacitance is decremented by an inverse multiplication factor of 1.1 until reaching the lower limit of 0.50 pF. The contour plot is logarithmic and describes the frequency response with a maximum at 875 kHz and a minimum at 0.785 Hz. Appendix B contains a thorough explanation of the contour plots including tables which assist in determining the results.

The noise calculations were performed in both the Basic and Fortran computer languages. Basic was used to generate the Bode diagrams, i.e., Figure 27. Fortran was used on the Cray to generate the contour plots. A complete listing of these programs can be found in Appendix C.

CHAPTER 5

TIME-DOMAIN ANALYSIS

The effects of the feedback resistor and capacitor on the bandwidth of the system were demonstrated in the preceding section. Since the signal is integrated following the detection and amplification stage, it is of interest to determine the effects of these components on the actual signal. Information about the time-domain signal can help in the selection of integration times and discrete components in order to capture the maximum amount of signal.

The return light signal from the fluorescent dye is related to the intensity and duration of excitation from the flashlamp. The flashlamp produces a short pulse of light, on the order of microseconds, which excites the dye for effectively the same amount of time. Following excitation, the fluorescent dye has emission characteristics which can be described by at least three decaying exponentials. The effective time constants for this decay are on the order of nanoseconds and is negligible compared to the duration of the flashlamp. Therefore the emission characteristics follow the excitation characteristics of the flashlamp.

The signal can be represented by its Fourier components. These components are described by an infinite sum of sine and cosine functions of differing amplitudes and frequencies. Since the signal is a short burst of energy resembling a pulse, there are high frequency components present. The feedback resistor-capacitor combination will have a filtering effect and will limit the higher order frequency components. As the higher order frequency components are lost the signal becomes more distorted, the amplitude is reduced and the signal

is more dispersed in time. A longer time interval would be necessary to retrieve the dispersed signal. The theoretical integration values can be calculated for different bandwidths and an optimal bandwidth can be derived.

The transfer function for the transconductance gain was derived in the preceding section and is described by Equation (4-10). It is a second-order equation and the poles can be determined using the quadratic equation. The poles are found to be at

$$p_1 = -b + \sqrt{\frac{b^2 - 4ac}{2a}} \qquad (5\text{-}1)$$

$$p_2 = -b - \sqrt{\frac{b^2 - 4ac}{2a}} \qquad (5\text{-}2)$$

where

$$a = R_p R_f C_p + R_p R_f C_f$$

$$b = w_o R_p R_f C_p + A_o w_o R_p R_f C_f + R_f + R_p$$

$$c = w_o R_f + A_o w_o R_p.$$

The poles are separated using partial fractions and the inverse Laplace transform is taken. The resulting equation is the time-domain response of the transconductance amplifier following a unity gain impulse function. The time-domain equation is given by

$$V_{out}(t) = K_1 e^{(p_1 t)} + K_2 e^{(p_2 t)} \qquad (5\text{-}3)$$

where

$$K_1 = Q / (p_1 - p_2)$$

$$K_2 = Q / (p_2 - p_1)$$

$$Q = - (A_o w_o R_f R_p) / a.$$

According to Equation (5-3) the time-domain response of an impulse function input is the sum of two decaying exponentials. At zero time the output voltage is zero volts as can be seen from the values of K_1 and K_2, which are of equal magnitude but opposite in sign. As time increases the two exponentials decay at different rates creating a curve similar to that shown in Figure 32. As time approaches infinity the output voltage approaches zero.

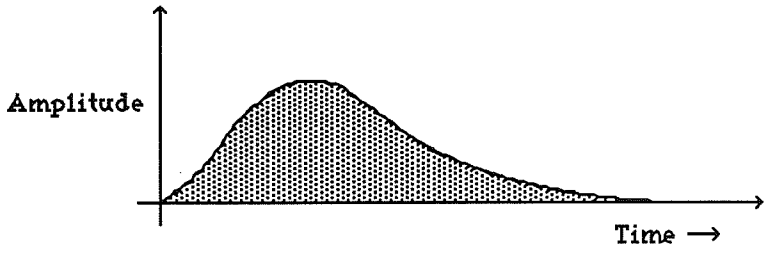

Figure 32 The time-domain response of the transconductance gain amplifier following a delta function input.

Equation (5-3) describes an overdamped system. There are two other possibilities which may exist. If the equality (b^2-4ac) in Equations (5-1) and (5-2) is less than zero then the system will be underdamped. If, on the other hand, (b^2-4ac) is equal to zero, the system will be critically damped. Since it would be rare that the components are chosen such that the poles are exactly identical, only

Solving for the underdamped case is similar to solving for the overdamped case but is slightly more complex. Partial fractions are determined for the complex poles and the corresponding terms are separated. The inverse Laplace transform is taken and the result is described in Equation (5-4).

$$V_{out}(t) = \frac{Q}{\beta} e^{-\alpha t} \sin(\beta t) \qquad (5\text{-}4)$$

where α is the real component and ß is the imaginary component of the pole.

Both Equation (5-3) and (5-4) can be integrated over a certain time interval. Equation (5-5) when integrated yields Equation (5-6) and in like manner Equation (5-7) following integration yields Equation (5-8).

$$A_1(t) = \int_0^{t_1} K_1 e^{(p_1 t)} + K_2 e^{(p_2 t)} \, dt \qquad (5\text{-}5)$$

$$A_1(t) = \frac{K_1}{p_1} e^{(p_1 t)} + \frac{K_2}{p_2} e^{(p_2 t)} \qquad (5\text{-}6)$$

$$A_2(t) = \int_0^{t_1} \frac{Q}{\beta} e^{-\alpha t} \sin(\beta t) \, dt \qquad (5\text{-}7)$$

$$A_2(t) = \frac{Q}{\beta} \left[\frac{-\beta}{(\beta^2 + \alpha^2)} + e^{-\alpha t} \frac{\alpha \sin(\beta t_0) + \beta \cos(\beta t_0)}{(\beta^2 + \alpha^2)} \right] \qquad (5\text{-}8)$$

A time period of 0.025 seconds corresponds to a flash frequency of 40 Hz. A frequency of 40 Hz was generally used during the experimentation and could give an indication of the signal amplitude following integration. The actual integration

time is 25 μsec. This integration interval is small and if it were used in the analysis it would lower the values for the integrated signal caused by a chopping of the trailing end of the dispersed signal.

The Equations (5-6) and (5-8) can be used to determine the magnitude of the actual signal following integration. These equations are used with different values of resistance and capacitance in a similar technique as was described in the previous section. A contour map of the magnitude of the signal following integration is generated and shown in Figure B-2. Note that there is a constant value of integration at the higher frequencies regardless of the feedback capacitor chosen. This implies that within this region the filtering effects will have no effect on the integrated signal. In other words, although the signal is lower in amplitude and dispersed in time, the actual area under the curve is the same.

CHAPTER 6

NOISE ANALYSIS

Within any system there are multiple sources of noise. This noise is especially noticeable in systems involving the detection of low level signals. Noise represents random electromagnetic fluxuations occupying the same spectral region as the signal.[1 2] In determining the noise present within a system, the system is broken down into its discrete components. The noise for each component is determined separately and combined to give the total noise of the system. Noise is summed according to the equation

$$N_t = \sqrt{N_1^2 + N_2^2 + N_3^2 + N_4^2 + N_5^2 + \cdots\cdots} \qquad \textbf{(6-1)}$$

where N_k describes the individual noise contributions and N_t describes the total noise of the system.

The noise present within each individual component is usually given in terms of a noise spectral density. The spectral density $(S(\nu)_n)$ describes the noise power across the whole frequency spectrum. In order to convert the noise power within a certain bandwidth into a noise voltage or current within the same bandwidth Equation (6-2) is used.

$$n_{vi} = \sqrt{\int (S(\nu)_n)^2 \, dt} \qquad \textbf{(6-2)}$$

Equation (6-2) is very similar to Equation (6-1). Since the spectral density can be described as a continuous function, an integral can be used to determine the noise whereas Equation (6-1) deals with the discrete addition of noise components.

The major sources of noise within an electrical system include thermal noise, dark current, shot noise and amplifier noise. By understanding the sources of noise and the relative contribution each makes to the total noise, an optimum design for the system can be achieved. Before proceeding to the actual analysis of the noise within the operational amplifier - photodiode pair, a brief explanation of the shot noise, Johnson noise and 1/f noise is presented.

6.1 Shot Noise Derivation

Shot noise is caused by the discreteness of the arrival of charge carriers on the photodetector. The arrival of the incident photons can be described by a Poisson distribution.[7] Shot noise is a fundamental limitation of any system since it is in principle even present at a temperature of absolute zero (-273 ^{o}C). Quantum-limited detection is defined as measurements taken within the limit of the shot noise, since the sensitivity of these measurements is described by the Heissenburg uncertainty principle.

A complete description of the derivation of shot noise can be found in References 7, 12 and 13. A brief description of this derivation is given presently. Consider a single electron within the depletion layer of a pn junction which has a length d; recall Figure 8. An in-coming photon strikes the electron causing it to be released. The electron is free and excited and will move toward the anode at a

velocity $v_e(t)$. The transit time of an electron was given in Equation (2-2). Using the relation

$$\text{Current} = \frac{\text{Charge}}{\text{time}} \tag{6-3}$$

the current generated due to the single electron can be calculated. The current pulse due to this electron is described by

$$i_e(t) = \frac{e\, v_e(t)}{d} \tag{6-4}$$

Consider that the photon strikes the electron at time t = 0 and it reaches the anode at time t = t_1. In order to derive the spectral density of the shot noise, the Fourier transform of the single current pulse is given by[12]

$$F(\omega) = \int_0^{t_1} i_e(t)\, e^{-i\omega t}\, dt \tag{6-5}$$

Substituting Equation (6-4) into Equation (6-5) yields the relation

$$F(\omega) = \int_0^{t_1} \frac{e}{d}\, v(t) e^{-i\omega t}\, dt \tag{6-6}$$

Since transit time t_1 of the electron is extremely small, the term $\omega t_1 << 1$. Therefore the term $e^{-j\omega t}$ is very close to unity. The Fourier transform then becomes

$$F(\omega) = \int_0^{t_1} \frac{e}{d} \frac{dx}{dt} dt \qquad \textbf{(6-7)}$$

where the velocity of the electron $v_e(t)$ is constant between the time t=0 and $t=t_1$. Solving for the integral yields

$$\frac{e}{d} x t \Big|_0^{t_1} \qquad \textbf{(6-8)}$$

and $x(t_1)$ is equal to d by definition. The Fourier transform is then found to be equal to e. In other words, a single current pulse generated by an incident photon can be described by an impulse function of amplitude e. Thus, in the frequency domain, the function is not band-limited and has a constant amplitude e. The definition of the spectral density function is given by Carson's theorem and is shown in Equation (6-9).[14]

$$S(\nu) = 2 N_{avg} |F(\omega)|^2 \qquad (6\text{-}9)$$

The value N is equal to the average rate of electron emission within the depletion region. The average rate of emission is determined by the average current due to the flow of electrons within the depletion region (I_{avg}) divided by the electron charge. This can be described by the relation

$$N_{avg} = \frac{I_{avg}}{e} \qquad \textbf{(6-10)}$$

Using the Equations (6-8), (6-9) and (6-10) the current spectral density within the depletion region of a pn junction can be shown to be

$$S(\nu) = 2\, e\, I_{avg} \qquad \textbf{(6-11)}$$

The spectral density describes the power within the whole frequency spectrum. In order to describe the power within a certain bandwidth of frequency, the bandwidth of interest is included in the equation according to Equation (6-2). Considering an average current which is constant in time, the rms amplitude noise current can be described by

$$i_n = \sqrt{2\, e\, I_{avg}\, B} \qquad \textbf{(6-12)}$$

where B is the bandwidth defined by the limits of integration in Equation (6-2).

Equation (6-13) describes the rms current due to the shot noise of the system. The variable x is defined as

$$I_{avg} = I_d + I_L \tag{6-13}$$

where

I_d = Current flow through the photodiode in the absence of light.

I_L = Current flow induced by light flux.

6.2 Shot Noise Analysis

Equation (6-13) can be used to determine the shot noise of the photodiode circuit shown in Figure 20. The current flowing through the pin photodiode is dependent on the light incident on the device. As the light level increases, the current through the photodiode also increases. The increased current corresponds to an increase in the shot noise of the photodiode. With no incident light on the photodiode there is a small current present known as the dark current. The dark current for the Hamamatsu S1722-01 photodiode is determined from the data to be $1x10^{-13}$ A.[14] This value is used to determine the absolute noise level of the system in the absence of light. The shot noise current of the photodiode is amplified along with the signal. Both the gain and the bandwidth are determined by the characteristics of the transconductance amplifier. A surface plot is generated describing the shot noise of the photodiode. Different values of the feedback resistor and capacitor were used to give an idea of the region of maximum noise.

This surface plot is shown in Figure 33. The maximum shot noise following amplification is found to be 4.61 uV and the minimum is 2.7 nV.

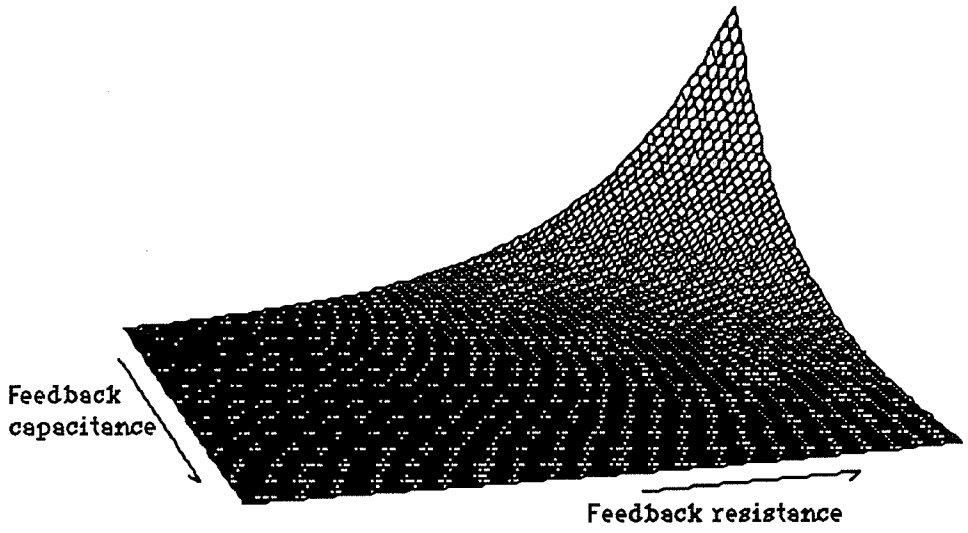

Figure 33 Surface plot of the shot noise.

6.3 Johnson Noise Derivation

Thermal or Johnson noise is caused by thermally agitated charge carriers within a resistive element. The Johnson noise can be modelled using the following parallel resistor circuit shown in Figure 34. The noise current generated in R_1 will flow through both R_1 and R_2. Since the resistors are matched there will be a maximum power transfer between the two resistors. The measureable noise energy due to R_1 is

$$E = k\,T \qquad \textbf{(6-14)}$$

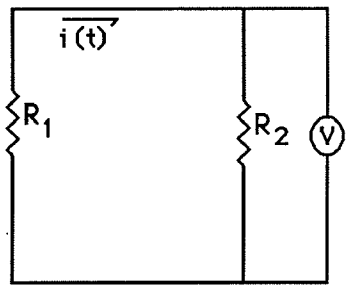

Figure 34 Resistor circuit network used to model the Johnson noise of a resistor.

Half of this noise energy, however, is dissipated in R_1 while the other half is dissipated in R_2. The resistor R_2 is considered the resistive element within the measurement device. The noise power (power=energy/time) generated by R_1, having a time constant of $\Delta\tau$, is described by

$$P_j = \frac{k\,T}{2\Delta\tau} \qquad \textbf{(6-15)}$$

The effective bandwidth of a circuit is equal to reciprocal of twice the time constant.

$$B = \frac{1}{2\Delta\tau} \qquad \textbf{(6-16)}$$

so Equation (6-15) can be rewritten as

$$P_j = k\,T\,B \qquad \textbf{(6-17)}$$

The voltage noise generated in R_1 will be distributed through both R_1 and R_2 as described above. The voltage across R_2 can be described using a simple voltage divider and is shown to be

$$V_{R2} = \frac{V_j R_2}{(R_1 + R_2)} \qquad \textbf{(6-18)}$$

The power dissipated across a resistor can also be described by Equation (6-19).

$$P_{rms} = \frac{(V_{R2})^2}{R_2} \qquad \textbf{(6-19)}$$

Considering that the impedances are matched ($R_1 = R_2$), the Johnson noise voltage can be calculated using (6-17), (6-18) and (6-19). The resulting equation is

$$V_j = \sqrt{4\,k\,T\,R\,B} \qquad \textbf{(6-20)}$$

The Johnson noise current can also be solved for in a similar fashion using the equation

$$P_j = V_j\, I_j \qquad \textbf{(6-21)}$$

The equation for the Johnon noise current generated in a resistor of value R is

$$I_j = \sqrt{\frac{4\,k\,T\,B}{R}} \qquad \textbf{(6-22)}$$

6.4 1/f Noise Discussion

As the noise power spectrum reaches the lower frequencies there is an additional noise element known as 1/f noise. The cause of 1/f noise is not well known, but may be related to a lack of ohmic contact at the connections within the circuit.[15] A model of the 1/f noise can be approximated empirically by the expression

$$i_{rms} = a\sqrt{\frac{I_b^{\beta} B}{f^{\alpha}}} \qquad (6\text{-}23)$$

where the terms are defined as:

a = proportionality constant

I_b = current through the detector

$\alpha \sim 2$

$\beta \sim 1$

B is the frequency bandwidth

f is the frequency operating point

The 1/f noise spectral density decreases at a rate of 10 dB per decade until reaching about 10 Hz. At 10 Hz the noise contribution from other elements dominates the noise characteristics of the device. Photovoltaic detectors generally have a negligable 1/f noise current.[7]

In order to determine the total output voltage noise of the circuit shown in Figure 20, the circuit is sub-divided into its major noise elements. The noise generated from each of the components can then be summed according to Equation (6-1).

6.5 Current Injection Circuit Noise Analysis

The current injection circuit is shown attached to the inverting input of the operational amplifier in Figure 20. Since the transconductance gain of the amplifier is $1x10^7$, any small dc currents present at the inverting input of the operational amplifier will appear as a large offset voltage at the output. The purpose of the current injection circuit is to provide a means to correct any dc offsets generated by the operational amplifier.

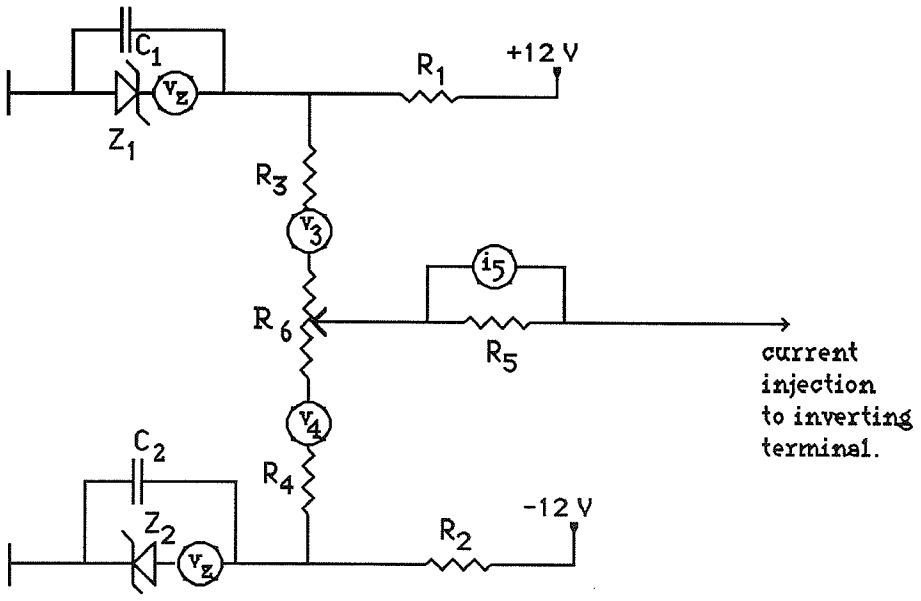

Figure 35 Current injection circuit with noise sources.

The current injection circuit consists of zener diodes and resistive elements which are capable of introducing a noise current at the inverting input of the operational amplifier. This noise current will contribute to the total noise of the system. Figure 35 describes the current injection circuit including the noise sources associated with each of the discrete components. The zener diodes have capacitors C_1 and C_2 to filter the noise voltage generated at the stable reference points. The filter is described as a low-pass filter with a pole at 796 Hz. Considering that noise spectral density of the Motorola 1N829A zener diodes has an increased noise power at the higher frequencies, a pole at 796 Hz will limit the noise effects considerably.[15]

A voltage noise generated by the zener diode will manifest itself as a current through resisor R_5. Using circuit analysis the current through the resistor R_5 is calculated to be

$$I_z = \frac{V_{zn}}{R_5}\left[\, 1 - \frac{xR_6 + R_3}{(R_3 + xR_6) + \dfrac{((1-x)R_6 + R_4)R_5}{(1-x)R_6 + R_4 + R_5}} \,\right] \qquad (6\text{-}24)$$

This current will sum at the inverting terminal of the operational amplifier according to Equation (6-1) and will be amplified by the transconductance amplifier. The noise is calculated for the zener diode with a constant noise spectral density of 0.1 uV/$\sqrt{}$Hz. This value allows a worst case situation for the noise of the zener diode. A contour plot of the noise levels at the output of the transconductance gain amplifier due to noise generated by the zener diode is shown in Figure B-3. The maximum and minimum noise levels were calculated to be 1.04 mV and 0.50 mV, respectively.

A similar calculation can be determined for each of the resistor elements within the circuit. The Johnson noise voltages of resistors R_3 and R_4 are represented by v_3 and v_4 in Figure 35. These resistors are matched and so the noise voltages of these two elements are similar. It was determined that the variations within the potentiometer R_6 play an insignificant role in the noise voltage differences between v_3 and v_4. The noise current at the input of the operational amplifier due to the noise voltage v_3 is described by Equation (6-25).

$$I_{R3} = \frac{\sqrt{4kTR_3B}}{R_5\left[1 + \frac{(1-x)R_6}{R_5} + \frac{(1-x)R_6}{(R_3+xR_6)}\right]} \qquad \textbf{(6-25)}$$

The final noise element within the current injection device is the Johnson noise of the resistive element R_5. This element will contribute a noise current which is defined by Equation (6-26).

$$I_{R5} = \sqrt{\frac{4kTB}{R_5}} \qquad \textbf{(6-26)}$$

Equations (6-24), (6-25) and (6-26) can be summed according to Equation 6-1 to derive the total noise of the current injection device, Equation (6-27).

$$I_{inj} = \sqrt{2 \times (I_{inj1})^2 + 2 \times (I_{inj3})^2 + (I_{inj5})^2} \qquad \textbf{(6-27)}$$

Equation (6-27) can be used to determine the values of R_3, R_4, and R_5 which can be used without being a dominant component of the noise voltage. The values of R_3, R_4, and R_5 are incremented between 1 kΩ and 100 MΩ to determine the noise levels at the output of the transconductance gain amplifier. The results are shown in Table 1.

Table 1 The output voltage noise due to different values of resistors within the current injection circuit.

	R_5					
R_3	1k	10k	100k	1M	10M	100M
1k	1.6591E-02	5.2313E-03	1.6293E-03	5.1393E-04	1.6247E-04	5.1378E-05
10k	1.9889E-02	6.4887E-03	1.7075E-03	5.1663E-04	1.6256E-04	5.1380E-05
100k	4.1321E-02	1.5710E-02	2.6498E-03	5.5822E-04	1.6394E-04	5.1424E-05
1M	.1221	4.8552E-02	7.0763E-03	8.8403E-04	1.7782E-04	5.1884E-05
10M	.3833	.1532	2.1932E-02	2.3421E-03	2.8122E-04	5.6276E-05
100M	1.211	.4844	6.9214E-02	7.2476E-03	7.4414E-04	8.8982E-05

One further consideration that must be taken before determining the component values of the current injection circuit is the sensitivity required to adjust the current injected at the inverting terminal of the operational amplifier. When the resistor R_6 is small compared to resistors R_3 and R_4, the major voltage drop of the reference voltage is across R_3 and R_4. This would allow small voltage variations as the potentiometer is adjusted. Resistor R_5 converts the voltage at the potentiometer into a current which is present at the inverting terminal of the operational amplifier. To maximize the sensitivity, large value resistors for R_3, R_4,

and R_5 should be used. To minimize the noise, a large value for R_5 should be used and small values for R_3 and R_4. The actual values used in the circuit are:

$R_3 = 2\ M\Omega$

$R_4 = 2\ M\Omega$

$R_5 = 22\ M\Omega$

Using these values the total noise of the current injection circuit at the output of the transconductance gain amplifier can be calculated. This is done for the different values of feedback resistors and capacitors as described earlier. The maximum and minimum Johnson noise voltages due to the resistor elements R_3 and R_4 are 16.5 uV and 0.081 uV, respectively. The maximum and minimum Johnson noise voltages due to the resistor element R_5 are 74.2 uV and 0.36 uV. A contour plot of the total noise within the current injection circuit is shown in Figure B-4. The maximum noise level for the circuit is 1.66 mV, while the minimum is 0.81 uV.

6.6 Operational Amplifier Noise Analysis

Within a transconductance amplifier network there are two major sources of noise that add to the total output noise voltage. The first of these is the noise inherent within the operational amplifier itself, and the second source of noise is the Johnson noise produced by the feedback resistor R_f.

The noise model for determining the amplifier noise gain of the circuit in Figure 20 is shown in Figure 36. Both voltage and current noise contribute to the total noise at the output. The circuit of Figure 36 can also be used to determine the dc output voltage shift due to the input offset voltage and the input bias current. In this case the capacitors C_1 and C_2 do not enter into the solution and the circuit can be solved to yield

$$V_{out} = V_n \left[1 + \frac{R_f}{R_p} \right] + I_n R_f \qquad \textbf{(6-28)}$$

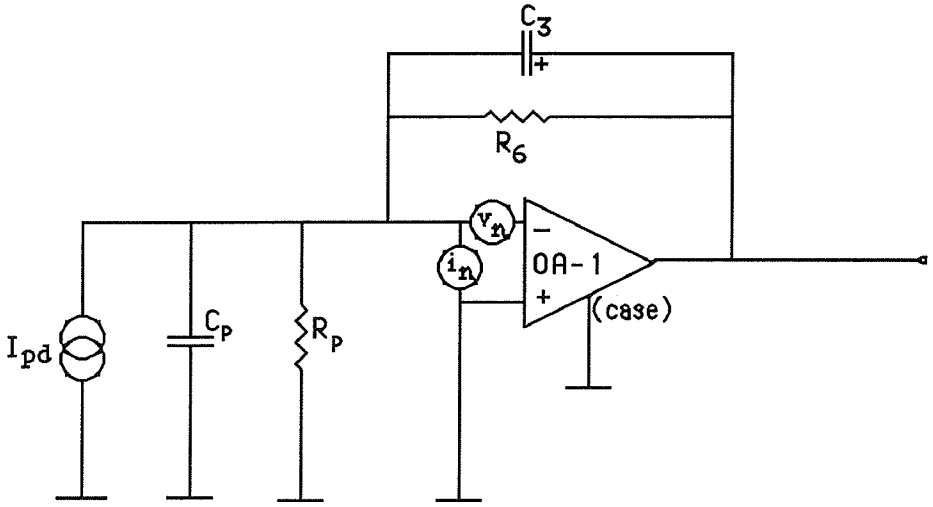

Figure 36 Operational amplifier model with noise sources included.

The maximum input offset voltage of the OPA101 is 0.6 mV and the maximum input bias current is 15 pA. The maximum offset voltage at the output is then 2.75 mV. This offset, however, can be adjusted to zero using the current injection circuit.

Considering that the voltage and current elements in Figure 36 are noise elements, an equation for the voltage noise gain and a current noise gain of the amplifier can be calculated. The noise voltage gain is considered first. Applying superposition, the current noise source is replaced with an open circuit. An equation for the voltage noise gain of the operational amplifier is determined to be

$$\frac{V_{out}}{V_{in}} = \frac{[R_p(1+sR_fC_f)R_f+(1+sR_pC_p)]}{R_p(1+sR_fC_f)} \qquad \textbf{(6-29)}$$

Substituting the equality $s=j\omega$ and solving for the real and imaginary terms, the voltage noise gain can be determined as a function of frequency. The voltage noise gain of Figure 36 is then ploted as a fuction of frequency as shown in Figure 41. Equation (6-29) is valid in the lower frequency spectrum; however, at higher frequencies the gain should drop to zero due to the effect of the open loop operational amplifier pole. In order to accurately model the noise gain at higher frequencies the open loop gain of the operational amplifier must be taken into account. The open loop gain is defined by Equation (6-30).

$$\frac{V_{out}}{V_{in}} = \frac{A_o}{[1+s/W_o]} \qquad \textbf{(6-30)}$$

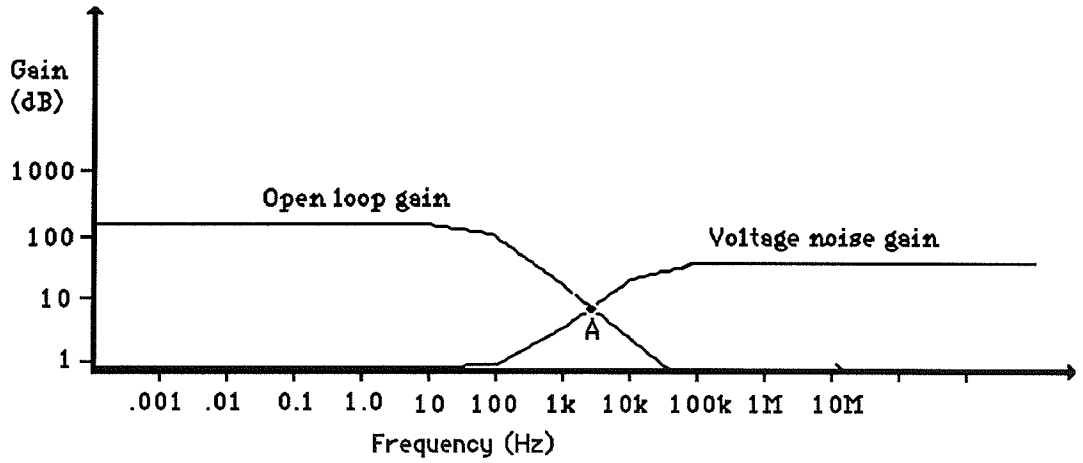

Figure 37 Plot of the open loop gain and the noise voltage gain of the operational amplifier.

Figure 37 is a plot of the open loop gain and the voltage noise gain of the operational amplifier both with respect to frequency. The point of intersection of the open loop gain and the noise amplifier gain can clearly be identified as point A. The actual noise gain of the amplifier will be defined by Equation (6-29) up to point A. Following this point the noise amplifier gain will be defined by the open loop gain of the amplifier. In order to combine these two equations, it can be seen that there must be an additional pole in Equation (6-29) which is defined at the point A, Figure 37. This pole can be determined by finding the intersection of the open loop gain and the noise voltage gain equations and setting a pole at that frequency. The following constraint must hold

$$A = s \left| \frac{A_o}{[\,1 + s/W_o\,]} = 1 + \frac{(1 + s R_p C_p)}{(1 + s R_f C_f)} \right. \qquad (6\text{-}31)$$

Solving for s, or the point of intersection, yields a quadratic equation in s. The actual point of intersection is then determined to be

$$p_1 = -b - \sqrt{\frac{b^2 - 4ac}{2a}} \qquad \textbf{(6-32)}$$

where

$$a = R_p R_f C_f + R_f R_p C_p$$

$$b = R_p + R_f + w_o (R_p R_f C_f + R_f R_p C_p) - A_o w_o R_p R_f C_f$$

$$c = (R_p + R_f) w_o - A_o \, wo \, R_p$$

The solution for A describes a pole which lies on the real axis in the frequency domain. This pole is included in Equation (6-29) and the real and imaginary parts of this new equation are calculated. The real and imaginary parts are then used to calculate the magnitude of noise gain as a function of frequency. This is plotted in Figure 38 and is defined as the noise gain spectral density of the OPA101AM. The input voltage noise of the operational amplifier, Figure 36, has not yet been introduced into the analysis. The input voltage noise has a specific spectral density which is characteristic of the amplifier and is shown in Figure 39. This figure was given in a Burr Brown data book describing characteristics of the OPA101AM.[16] It can be modelled using Laplace techniques to attain Equation (6-33)

$$s\,(v) = \frac{8\,nV}{\sqrt{Hz}} \, \frac{(s + Z_5)}{\sqrt{s}} \qquad \textbf{(6-33)}$$

where the zero $Z_5 = 2\pi(100 \text{ Hz})$.

The noise spectral density is considered the voltage V_n of Figure 36. In order to determine the output noise spectral density, the input noise voltage spectral density and the operational amplifier and the voltage noise gain spectral density are multiplied together. The result of this multiplication (Equation (6-34)) describes the output noise characteristics of the OPA101AM operational amplifier. Again substituting the relation s=jw and solving for the real and the imaginary parts the output noise spectral density is plotted as output noise voltage versus frequency (Figure 40).

$$\frac{V_{out}}{V_{in}} = \frac{[R_p(1+sR_fC_f)R_f+(1+sR_pC_p)]}{R_p(1+sR_fC_f)(s+p_1)} \qquad (6\text{-}34)$$

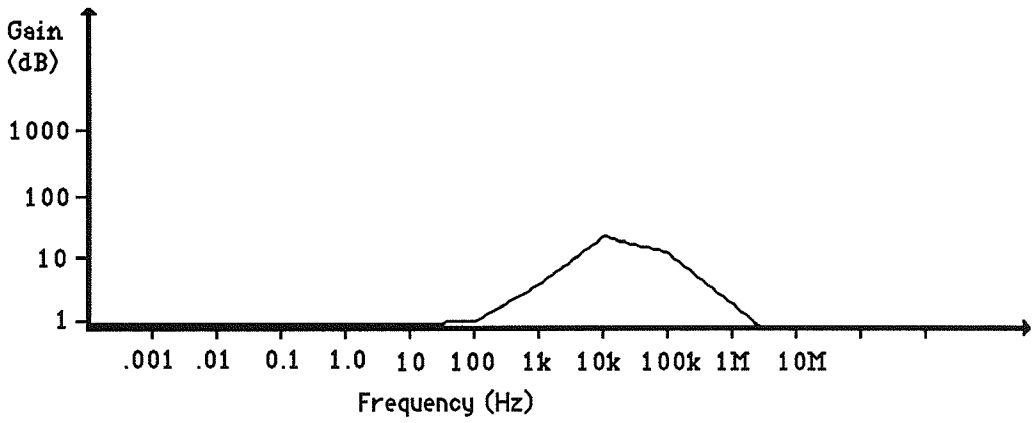

Figure 38 The voltage noise amplification for the amplifier operated in the current to voltage converter mode.

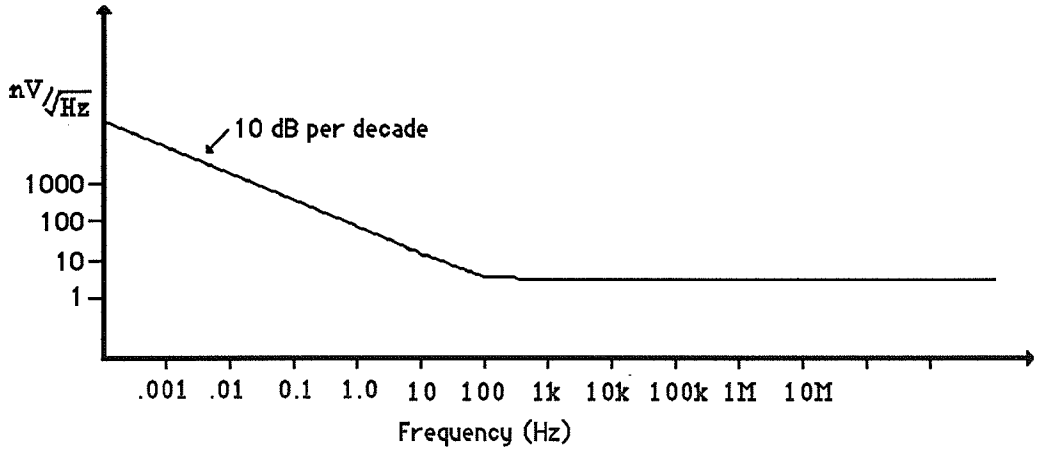

Figure 39 Input voltage noise spectral density of the Burr Brown OPA101Am operational amplifier.

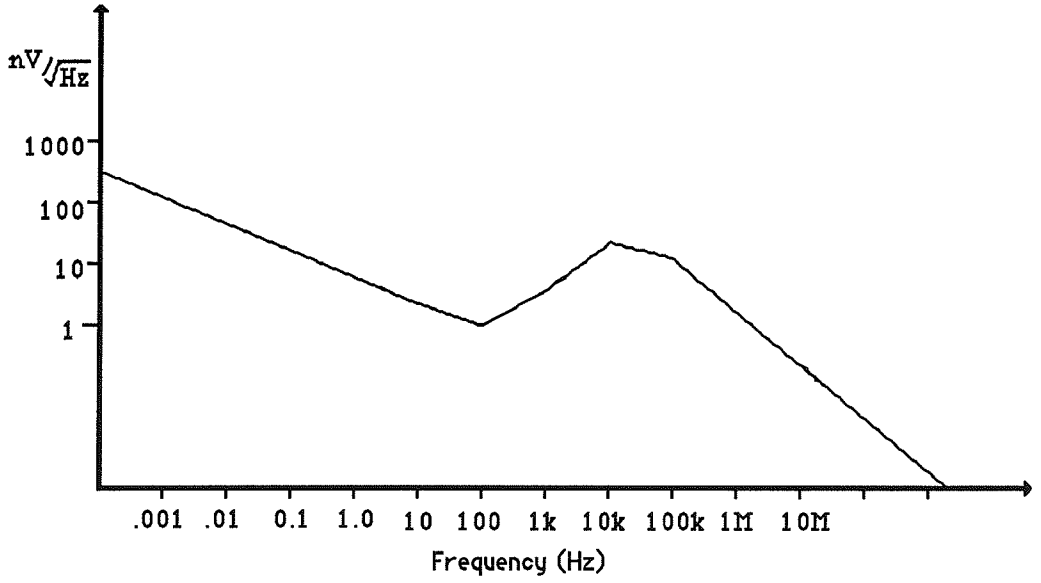

Figure 40 Output noise spectral density due to the input voltage noise of the operational amplifier.

Note from Figure 40 that there is an increase in the voltage noise gain at higher frequencies. This high-frequency gain is due to capacitive interaction between the feedback resistor (R_f) and the shunt capacitance of the photodiode (C_p).

The total rms amplifier noise at the output due to the voltage noise of the operational amplifier can be determined using Equation (6-2). The voltage noise spectral density of the operational amplifier is integrated over the entire frequency spectrum using computer integration techniques. Each segment of the integral is squared and multiplied by the integral segment dw. The segments are summed and upon completion the square root is determined. The noise of the amplifier can then be calculated using different values of feedback resistors and capacitors as before. The contour plot of the output voltage noise due to the input voltage noise of the operational amplifier is shown in Figure B-5. The maximum noise is determined to be 624 uV and the minimum noise voltage is 47.4 uV.

The output voltage due to the input noise current can be calculated in a similar fashion. The voltage noise source of Figure 36 is replaced with a short circuit and the voltage at the inverting terminal is thus considered a virtual ground. In this case, theoretically all noise current will flow through the feedback resistor.

The spectral density of the input noise current is determined from data for the OPA101. Using Laplace modelling techniques the transfer function for the input noise current is calculated to be

$$I_{in} = \frac{1.4\,fA}{\sqrt{Hz}} \quad (1 + \frac{s}{2\pi\,(10k\,Hz)}) \qquad (6\text{-}35)$$

The magnitude of the transfer function above is plotted in Figure 41. It can be seen that the current noise increased at 20 dB/decade beginning at 10 kHz. For large transconductance amplifier bandwidths this can play a significant role in the noise of the system.

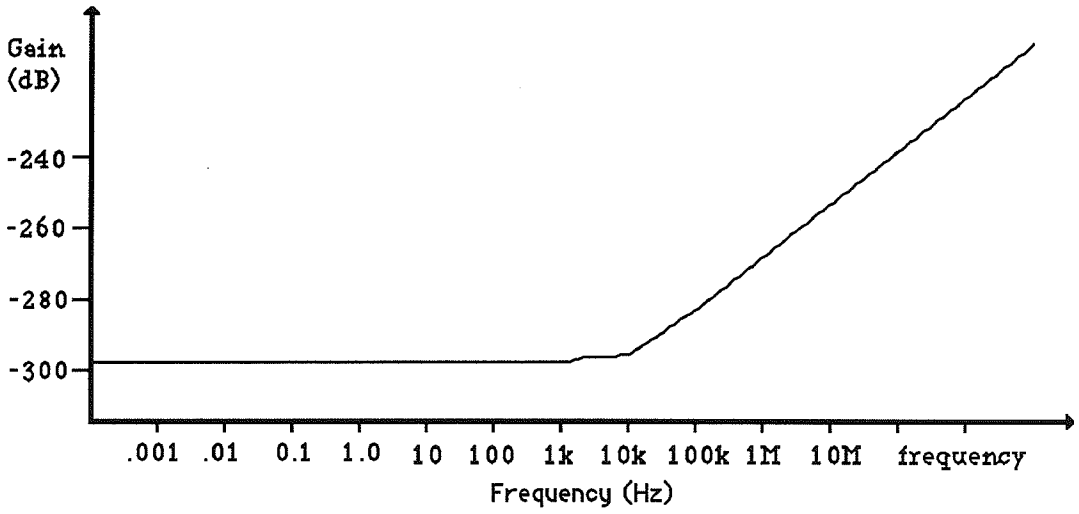

Figure 41 Input noise current spectral density of the operational amplifier.

The transconductance of the amplifier was determined in Chapter 4 and defined by Equation (4-10). The input noise current is used as the input current, I_{in}. Solving for the transfer function for the output voltage due to the input noise current yields

$$V_{out} = \frac{K_1 + s\,(K_1 / P_6)}{as^2 + bs + c} \qquad \textbf{(6-36)}$$

where

$K_1 = - A_o R_p R_f w_o$ (1.4 fA)

$P_6 = 2\pi$ (10 kHz)

and a, b and c, are defined the same as in Equation (5-1) and (5-2).

Substituting s = jw into the above equation, solving for the real and imaginary parts and determining the magnitude of the transfer function at different frequencies, a plot of output noise voltage versus frequency can be shown, Figure 42.

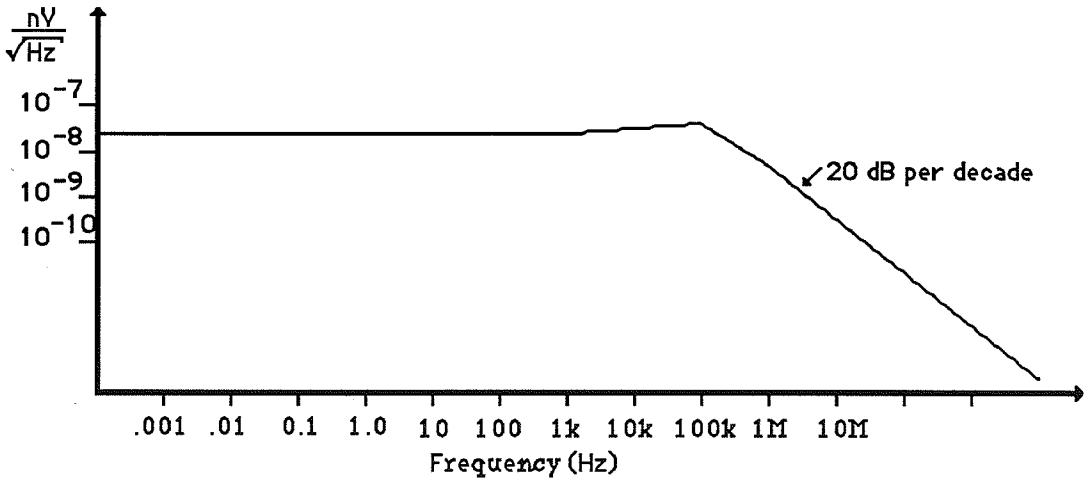

Figure 42 Output noise spectral density due to the current noise of the operational amplifier.

The total rms amplifier noise at the output due to the input current noise is generated in a similar fashion as previously demonstrated. Equation (6-36) is integrated over the entire frequency spectrum using computer integration techniques. Each segment of the integral is squared and multiplied by the integral segment dw. The summation over these segments follows and upon completion, the square root is taken. A contour plot of the output voltage noise due to the input current noise of the operational amplifier is given in Figure B-6. The maximum is 57.9 uV and the minimum is 0.3 uV.

The second source of noise associated with an inverting operational amplifier is the Johnson noise of the feedback resistor. The equation for Johnson noise derived earlier is

$$V_j = \sqrt{4\,k\,T\,R_f\,\Delta f} \qquad \textbf{(6-37)}$$

Substituting the proper values into the above equation, the output noise

component due to the Johson noise of the feedback resitor can be calculated. Different values of feedback resistors and capacitors are used and a contour plot is generated, Figure B-7. Note that the relationship between the noise levels and the feedback resistor remains relatively constant. The Johnson noise component of the feedback resistor is significant only when the feedback capacitance is small. Thus a small resistance and a small capacitance would have a greater bandwidth and thus a higher noise component. There will be an equal amount of noise when the bandwith is reduced and the feedback resistance increased. A surface plot of the output voltage due to the Johnson noise of the feedback resistor is shown in Figure 43.

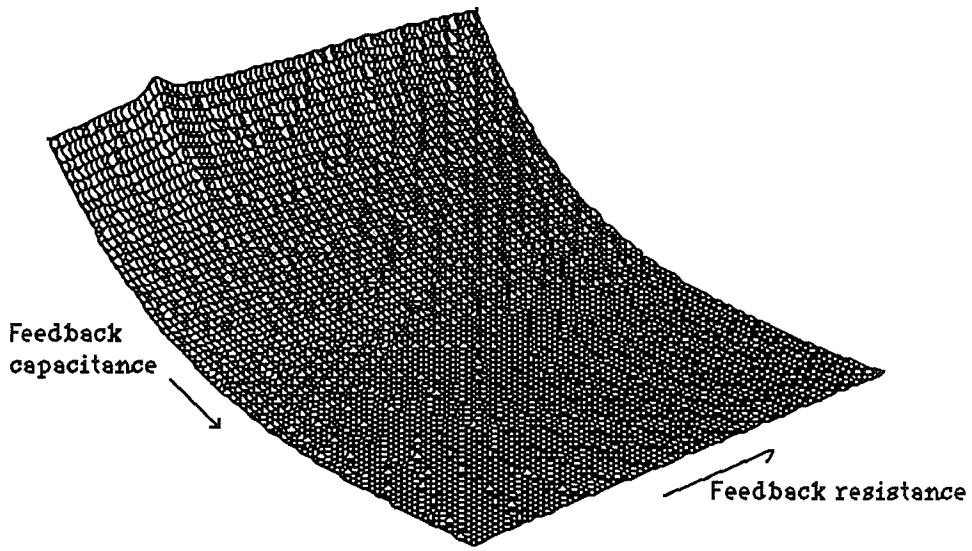

Figure 43 Surface plot of the Johnson noise of the feedback resistor.

6.7 Complete Noise Analysis Calculation

The total noise of the system is a combination of the individual noise elements summed according to Equation (6-1). The noise components discussed above include the shot noise of the photodiode, the noise present within the current injection

circuit, and the noise due to the operational amplifier. Both the current injection circuit and the operational amplifier sub-systems contain noise elements which are totalled to give the total noise associated within each of the sub-systems.

The total noise is calculated using the individual noise contributions which were calculated above. Each of these noise contributions is calculated in a Fortran program using the integration techniques described in Equation (6-2). The output voltage for each of the components is calculated and summed according to Equation (6-1). This is done for a range of feedback resistors and capacitors and the contour plot of the total noise of the system is shown in Figure B-8. The maximum noise of the system is determined to be 1.78 mV while the minimum is 47.7 uV.

The measured noise voltage at the ouput of the operational amplifier was obtained using a Hewlett-Packard 3478A multimeter. The total output noise of the system for different feedback resistor and capacitor combinations, both theoretical and experimental, are given in Table 2. The Hewlett-Packard 3478A multimeter specifies an accuracy between the range of 30 millivolts to 300 volts. Therefore, the experimental measurement values may be slightly different than the actual total noise values. The important point is that both the experimental and theoretical noise levels are approximately identical and follow the same pattern. There is an increase in total noise with increased gain and a decrease in total noise as the feedback capacitor is increased. The sensitivity of noise measurement was also limited by the internal noise of the multimeter. Since the noise of the multimeter and the output noise of the circuit are uncorrelated, they sum according to Equation (6-1). The noise of the multimeter is 520 uV and will dominate when the photodiode - operational amplifier circuit noise is below this level. The noise contribution of the HP 3478A multimeter was eliminated using

Equation (6-38),

$$(V_n)^2 = (V_{meas})^2 - (V_{HP})^2 \qquad \textbf{(6-38)}$$

where

V_n is the voltage noise at the output of the operational amplifier

V_{meas} is the actual measured voltage on the multimeter

V_{HP} is the noise floor of the multimeter (520 uV).

Table 2 Theoretical versus experimental noise results for different values of feedback resistors and capacitors.

		Feedback resistance (ohms)				
Theoretical		100 k	510 k	1 M	10 M	22 M
Feedback capacitance	0 pF	261 µV	296 µV	319 µV	447 µV	517 µV
	1 pF	203 µV	246 µV	271 µV	350 µV	400 µV
Experimental						
Feedback capacitance	0 pF	-	581 µV	568 µV	720 µV	783 µV
	1 pF	102 µV	179 µV	245 µV	319 µV	339 µV

CHAPTER 7

NOISE LIMITING OPTIMIZATION TECHNIQUES

Each element within the front end amplifier contributes to the total noise of the system. The total noise includes contributions that differ in their relative magnitude: thus, if one element is an order of magnitude larger than another noise element, then this noise source will dominate. The dominant noise source was determined in the previous chapter to be due to the input voltage noise of the operational amplifier. It was shown in Figure 44 that at higher frequencies there is a capacitive gain which amplifies the otherwise small operational amplifier voltage noise (8 nV/$\sqrt{}$Hz). One method which can be used to limit this noise is by adding a filtering capacitor C_f and limiting the bandwidth. Although the overall noise level will decrease following the addition of a filtering capacitor, the voltage noise remains the dominant noise source at the lower frequencies.

There are problems associated with limiting the bandwidth. For example, the signal will be smaller in amplitude and more dispersed in time, as was demonstrated in Chapter 5. This poses no problems with respect to the magnitude of the integrated signal, as long as the integration interval is lengthened to compensate. However, when the integration interval is extended, there are problems due to the offset drift currents overriding the signal. In other words, the amplitude of the signal is decreased by the addition of a filtering capacitor and it is more difficult to distinguish between the signal and current drift components. The goal, therefore, is to maximize both the gain and the frequency response and to minimize the noise voltage at the output of the transconductance amplifier.

Three plots generated on the Cray XMP can be useful in determining the values of R_f and C_f in order to limit the noise voltage while maintaining the frequency response of the system. These plots consist of the frequency response characteristics (Chapter 4), integration time characteristics (Chapter 5), and the total noise output voltage of the system (Chapter 6). When these three plots (32, 34 and 51) are overlayed, the different parameters of the system can be chosen and the other values will be determined correspondingly. If, for example, a frequency response of 20 kHz and a gain of $1x10^7$ is required, the line corresponding to 20 kHz frequency and $1x10^7$ gain intersect and set the feedback capacitor value and the noise level. Using this technique, a noise level can be chosen as the maximum allowable noise level. The gain is then chosen depending on the level of signal present at the photodiode. The feedback capacitor value and the frequency response will then be set by the determination of these initial parameters.

Since the fluorescent signal is on the order of several hundred picowatts, a gain of $1x10^7$ would allow an output voltage of several millivolts. In order to achieve a signal-to-noise ratio of 20 dB, the noise level should be below several hundred microvolts. In this case the noise level must lie within the shaded area of Figure B-9. Choosing a gain of $1x10^7$ requires the feedback capacitor to be 5.3 pF and the frequency response is 3.06 kHz.

A second technique can be used to generate a plot that combines the maxima of the three plots generated above. Since the desired result is to maximize both the

gain and the bandwidth while minimizing the noise, an equation can be derived to determine an optimized maximum. The equation is

$$P_{max} = (\text{Gain x Bandwidth}) / \text{Noise} \qquad (7\text{-}1)$$

The computer is used to generate a plot which calculates the P_{max} for each point in the three 81x81 matrices. This plot is shown in Figure B-10. Figure B-10 can then be used to determine an appropriate value for resistance and capacitance which maximizes these three parameters. The values chosen are 1.75 MΩ for the feedback resistor and 0.71 pF for the feedback capacitor. The noise level for this case is 388 uV and a frequency response of 149 kHz. It should be noted that the values were not weighted before the calculation was determined. Weighting of the values is useful to determine which variable is the most significant.

CHAPTER 8

DISCUSSION

Using circuit analysis techniques of the pin photodiode - operational amplifier pair, the output voltage noise can be calculated. The output voltage noise is a combination of the shot noise of the photodiode, Johnson noise of the current injection circuit, zener diode noise of the current injection circuit, Johnson noise of the feedback resistor, and both the current and voltage noise of the operational amplifier. These noise components combine to form the total noise of the analog front end. This noise is also present on the inverting terminal of the operational amplifier. The photodiode converts the light signal to a current and this signal is also present at the inverting terminal of the operational amplifier. The signal and the noise current sum and special techniques should be used to reduce the effects of this noise.

The maxima and minima of the noise levels of each of the noise components listed above are shown in Table 3. Figure B-8, which was discussed in Chapter 6, displays the total noise of the operational amplifier - photodiode pair at different gains and bandwidths. The noise due to the current injection circuit becomes the dominant noise source at the area on the contour plots corresponding to high gain and a small feedback capacitance, the upper right-hand corner of Figure B-8. This area describes the maximum noise seen in Table 3. The zener voltage noise was taken as a worst-case situation and the actual noise due to this device may be lower than indicated in Table 3. At the minimum noise point, the lower left region on the contour plots, the amplifier voltage noise becomes dominant.

The location on the contour plots where the noise magnitude of the current injection circuit is approximately equal to the noise due to the operational amplifier is found very close to the maximum point. This can be seen from the two contour plots, Figure B-4 and Figure B-8. The noise of the current injection circuit falls at a rapid rate when moving towards the minimum. The voltage noise of the operational amplifier, however, decreases at a much slower rate. Therefore, at all points on the contour plots, excluding the points near the maximum, the voltage noise of the operational amplifier is dominant.

Table 3 Table displaying the magnitude of the maximum and minimum noise levels of the noise elements in the front end circuit.

Noise element	Maximum (uV)	Minimum (uV)
Shot noise	4.61	0.0027
Johnson noise of R_f	244	5.15
Op amp input voltage noise	624	47.4
Op amp input current noise	57.9	0.300
Johnson noise of R_3	16.5	0.081
Johnson noise of R_4	74.2	0.364
Zener diode noise	1,041	0.502
Current injection circuit noise	1,665	0.807
Total front end noise	1,785	47.7

An optimization technique allows two of the four parameters describing the system to be chosen. These parameters consist of the gain, frequency bandwidth, noise and the feedback capacitor. Two of these parameters are independent and may be chosen; the remaining two, however, are set according to the chosen parameters. This analysis allows the user to determine which parameters are the most significant and design the system accordingly.

CHAPTER 9

CONCLUSIONS

Sensors which utilize fluorescent properties have definite advantages in the realm of physiological measurements. Fiber optic sensors are small and flexible and do not provide a conduction path for electrical currents to the patient. Furthermore, sensors may be developed to continuously measure substances which were once difficult to measure except through chemical analysis techniques following a blood sample, i.e. glucose. Sensors are being devised for the clinical measurement of pH, blood gases, glucose, and other physiological substances.

A fluorescent sensor that is currently being developed is capable of measuring both pH and temperature. This sensor would be useful in monitoring the pH and temperature during microwave-induced hyperthermia treatment of tumors. Conventional electrodes are unable to measure these properties due to the field effects associated with the measurements.

The design of the complete system is composed of three subsystems, namely, optical, sensor, and electronic. The optical system is designed such that there is a minimal amount of optical loss during the filtering and processing of the excitation and fluorescent signals. A light source is also a component of the optical subsystem and is chosen such that there is a maximum amount of light energy transferred to the sensor at the wavelength of interest.

The sensor should be designed such that the fluorescent dye is immobilized within the sensor. The sensor should also be constructed so that the analyte will have the ability to freely diffuse in and out of the sensor and interact with the

fluorescent dye. Finally, the sensor should be designed to allow a maximum amount of fluorescent signal to be coupled back to the detector.

The electrical subsystem should have the ability to detect the signal and process it such that a reliable measurement of the analyte concentration can be achieved. Losses within the optical and sensor subsystems create a situation in which the return light flux is weak. The measurement of weak light fluxes requires low noise component selection. In addition accurate measurements also require careful analysis to determine the operating point of these components.

The operating point of a photodiode - operational amplifier pair is determined by discrete components. These components, i.e., the feedback capacitor and feedback resistor, can be chosen to set the gain, maximum noise levels, and the frequency response of the system. If the intensity of the fluorescent emission can be determined, the light level at the photodiodes can be calculated by measuring the losses within the optical system. The magnitude of this signal is important in determining the gain and the absolute noise level of the front end circuit. Using optimization techniques discussed in Chapter 7, the values of the system components can be determined such that minimum noise and maximum gain can be attained.

If the signal noise level is too small to achieve a significant signal-to-noise ratio, then the next option is to use a photomultiplier tube. The advantage of a photomultiplier tube is that the gain is essentially noise free, whereas the noise gain of the operational amplifier is the dominant noise source.

APPENDIX A

COMPLETE CIRCUIT DIAGRAM

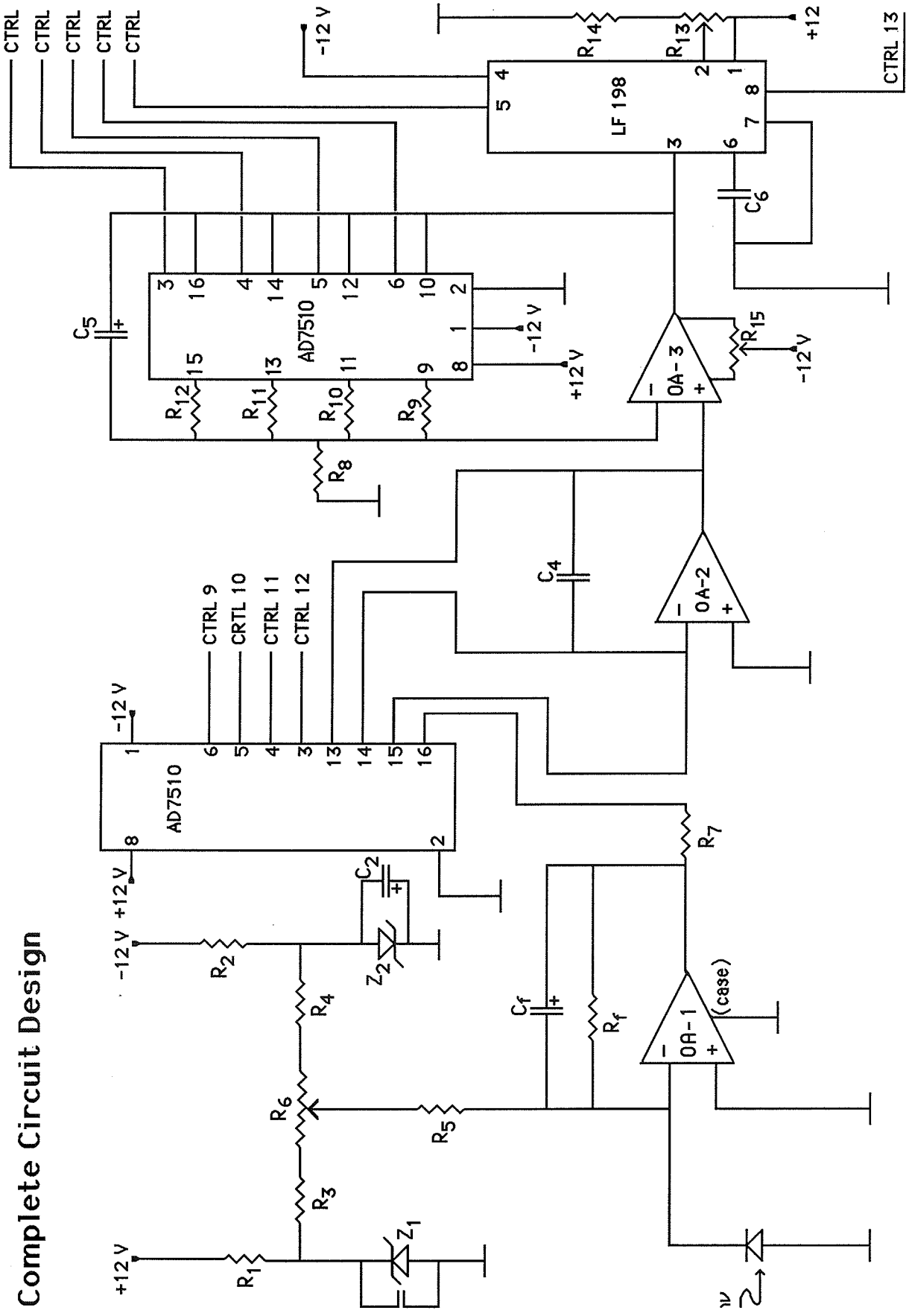
Complete Circuit Design
CTRL
CTRL
CTRL
CTRL
CTRL
-12 V
LF 198
R14
R13
+12
CTRL 13
C6
AD7510
C5
R12
R11
R10
R9
R8
+12 V
R15
OA-3
CTRL 9
CRTL 10
CTRL 11
CTRL 12
C4
OA-2
AD7510
C2
R7
R2
R4
Z2
Cf
Rf
OA-1
(case)
R6
R5
R3
R1
Z1
ν

APPENDIX B

CONTOUR PLOTS

Surface Plots

The surface plots were generated on the Cray XMP supercomputer at the University of Illinois at Urbana-Champaign. They consist of an 81 x 81 array of data points which are printed on a grid. The grid consists of 81 x 81 hash marks. The origin of these plots is in the lower left-hand corner and corresponds to the point $R_f = 1 \times 10^5$ and $C_f = 1 \times 10^{-9}$. Along the horizontal axis the resistance is incremented by a multiplicative factor of 1.1. This value was chosen to give a reasonable number of data points over the region of interest. The vertical axis consists of values for the feedback capacitor which decrement from the origin by an inverse multiplication factor of 1.1 (1.00/1.10). Table B-1 displays the hash mark values, point 1 being at the origin, corresponding to the resistance or capacitance at that point.

Each point on the contour plots is referenced logarithmically to the maximum. The maximum is shown on the plot as the maximum dB and all the other points decrease from this magnitude. At the bottom of the contour plots the following line can be seen

"CONTOUR FROM (value#1) TO (value#2) CONTOUR INTERVAL OF (value#3) PT(3,3) = (value#4)"

The values associated with this line are as follows:

value #1	The minimum point as referenced to the maximum (dB)
value # 2	The maximum point (dB)
value # 3	ΔdB per contour line
value # 4	Value at the origin

In order to convert the logarithmic levels shown on the contour plots into an actual noise level the following relation should be used:

$$dB = 20 \log (value\#5/max)$$

where value#5 is the actual noise level at a specific point on the contour plot. Table B-2 converts the dB readings to the actual frequency response (Figure B-1). Table B-3 relates the dB readings to actual noise values for the total noise of the system (Figure B-8).

Table B-1 A list of the values of resistance and capacitance associated with the hash marks on the contour plots. The value of resistance also corresponds to the gain.

Hash mark #	Resistance	Capacitance
1	1.0000E+05	1.0000E-09
2	1.1000E+05	9.0909E-10
3	1.2100E+05	8.2645E-10
4	1.3310E+05	7.5131E-10
5	1.4641E+05	6.8301E-10
6	1.6105E+05	6.2092E-10
7	1.7716E+05	5.6447E-10
8	1.9487E+05	5.1316E-10
9	2.1436E+05	4.6651E-10
10	2.3579E+05	4.2410E-10
11	2.5937E+05	3.8554E-10
12	2.8531E+05	3.5049E-10
13	3.1384E+05	3.1863E-10
14	3.4523E+05	2.8966E-10
15	3.7975E+05	2.6333E-10
16	4.1772E+05	2.3939E-10
17	4.5950E+05	2.1763E-10
18	5.0545E+05	1.9784E-10
19	5.5599E+05	1.7986E-10
20	6.1159E+05	1.6351E-10
21	6.7275E+05	1.4864E-10
22	7.4003E+05	1.3513E-10
23	8.1403E+05	1.2285E-10
24	8.9543E+05	1.1168E-10
25	9.8497E+05	1.0153E-10
26	1.0835E+06	9.2296E-11
27	1.1918E+06	8.3905E-11
28	1.3110E+06	7.6278E-11
29	1.4421E+06	6.9343E-11
30	1.5863E+06	6.3039E-11
31	1.7449E+06	5.7308E-11
32	1.9194E+06	5.2099E-11
33	2.1114E+06	4.7362E-11
34	2.3225E+06	4.3057E-11
35	2.5548E+06	3.9142E-11
36	2.8102E+06	3.5584E-11
37	3.0913E+06	3.2349E-11
38	3.4004E+06	2.9408E-11
39	3.7404E+06	2.6735E-11
40	4.1145E+06	2.4304E-11
41	4.5259E+06	2.2095E-11
42	4.9785E+06	2.0086E-11
43	5.4764E+06	1.8260E-11
44	6.0240E+06	1.6600E-11
45	6.6264E+06	1.5091E-11

46	7.2891E+06	1.3719E-11
47	8.0180E+06	1.2472E-11
48	8.8198E+06	1.1338E-11
49	9.7017E+06	1.0307E-11
50	1.0672E+07	9.3704E-12
51	1.1739E+07	8.5185E-12
52	1.2913E+07	7.7441E-12
53	1.4204E+07	7.0401E-12
54	1.5625E+07	6.4001E-12
55	1.7187E+07	5.8183E-12
56	1.8906E+07	5.2893E-12
57	2.0797E+07	4.8085E-12
58	2.2876E+07	4.3714E-12
59	2.5164E+07	3.9740E-12
60	2.7680E+07	3.6127E-12
61	3.0448E+07	3.2843E-12
62	3.3493E+07	2.9857E-12
63	3.6842E+07	2.7143E-12
64	4.0527E+07	2.4675E-12
65	4.4579E+07	2.2432E-12
66	4.9037E+07	2.0393E-12
67	5.3941E+07	1.8539E-12
68	5.9335E+07	1.6853E-12
69	6.5268E+07	1.5321E-12
70	7.1795E+07	1.3928E-12
71	7.8975E+07	1.2662E-12
72	8.6872E+07	1.1511E-12
73	9.5559E+07	1.0465E-12
74	1.0512E+08	9.5133E-13
75	1.1563E+08	8.6485E-13
76	1.2719E+08	7.8623E-13
77	1.3991E+08	7.1475E-13
78	1.5390E+08	6.4977E-13
79	1.6929E+08	5.9070E-13
80	1.8622E+08	5.3700E-13
81	2.0484E+08	4.8818E-13

Table B-2 The dB levels and the corresponding frequency response of the operational amplifier-photodiode pair.

Frequency response	dB
7.8500E+05	-.9428
6.2800E+05	-2.881
5.0240E+05	-4.819
4.0192E+05	-6.757
3.2154E+05	-8.696
2.5723E+05	-10.63
2.0578E+05	-12.57
1.6463E+05	-14.51
1.3170E+05	-16.45
1.0536E+05	-18.39
8.4289E+04	-20.32
6.7431E+04	-22.26
5.3945E+04	-24.20
4.3156E+04	-26.14
3.4525E+04	-28.08
2.7620E+04	-30.02
2.2096E+04	-31.95
1.7677E+04	-33.89
1.4141E+04	-35.83
1.1313E+04	-37.77
9050.	-39.71
7240.	-41.64
5792.	-43.58
4634.	-45.52
3707.	-47.46
2966.	-49.40
2373.	-51.34
1898.	-53.27
1518.	-55.21
1215.	-57.15
971.8	-59.09
777.4	-61.03
621.9	-62.97
497.6	-64.90
398.0	-66.84
318.4	-68.78
254.7	-70.72
203.8	-72.66
163.0	-74.59
130.4	-76.53
104.3	-78.47
83.48	-80.41
66.78	-82.35
53.42	-84.29
42.74	-86.22

34.19	-88.16
27.35	-90.10
21.88	-92.04
17.51	-93.98
14.00	-95.91
11.20	-97.85
8.963	-99.79
7.170	-101.7
5.736	-103.7
4.589	-105.6
3.671	-107.5
2.937	-109.5
2.350	-111.4
1.880	-113.4
1.504	-115.3

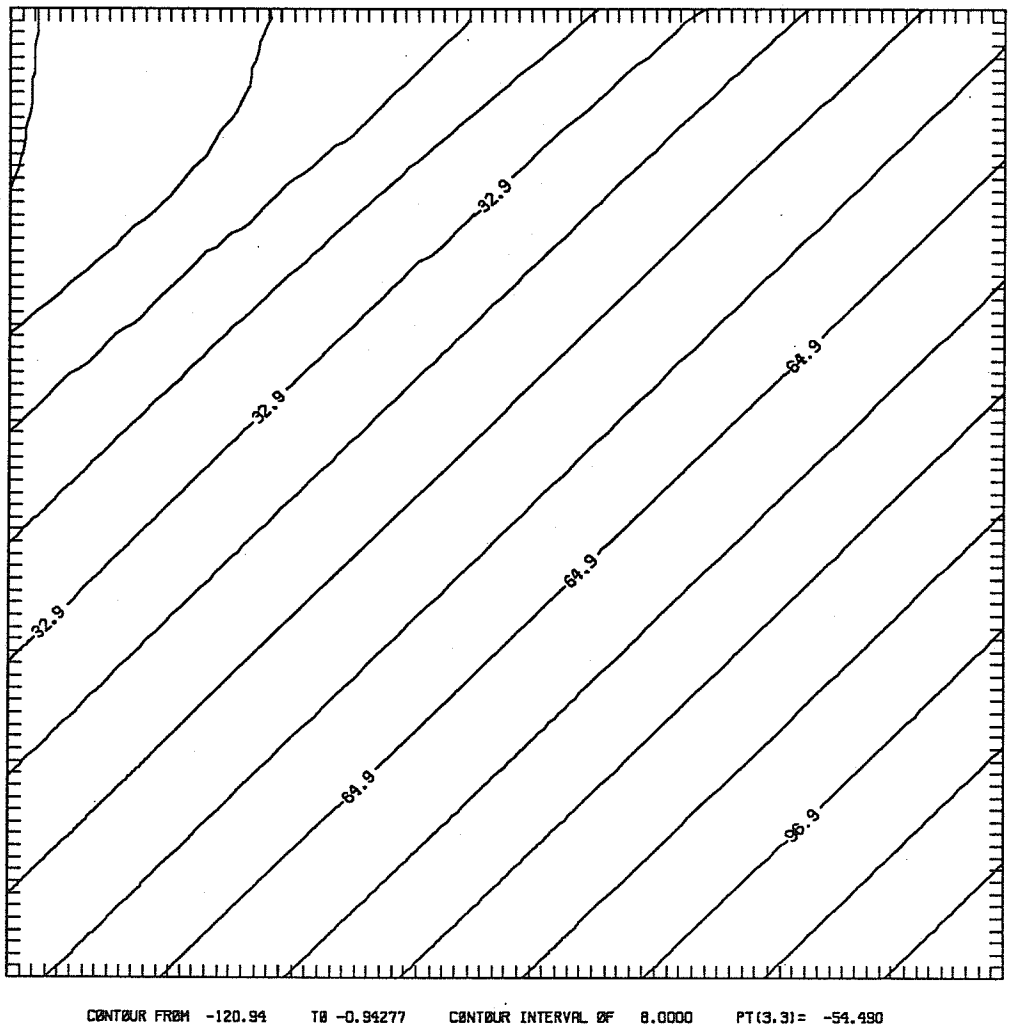

Figure B-1 Contour plot of the frequency response of the operational amplifier-photodiode pair.

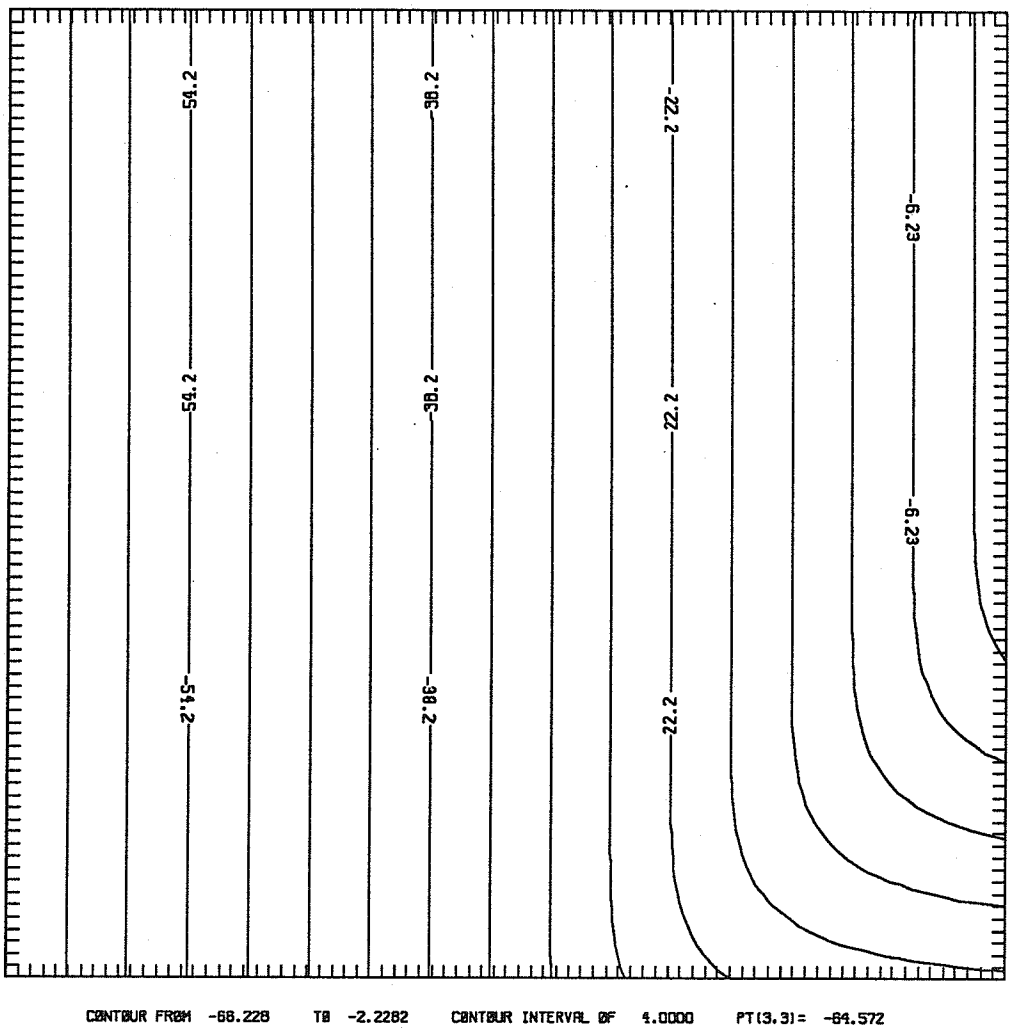

Figure B-2 Contour plot of the integrated signal.

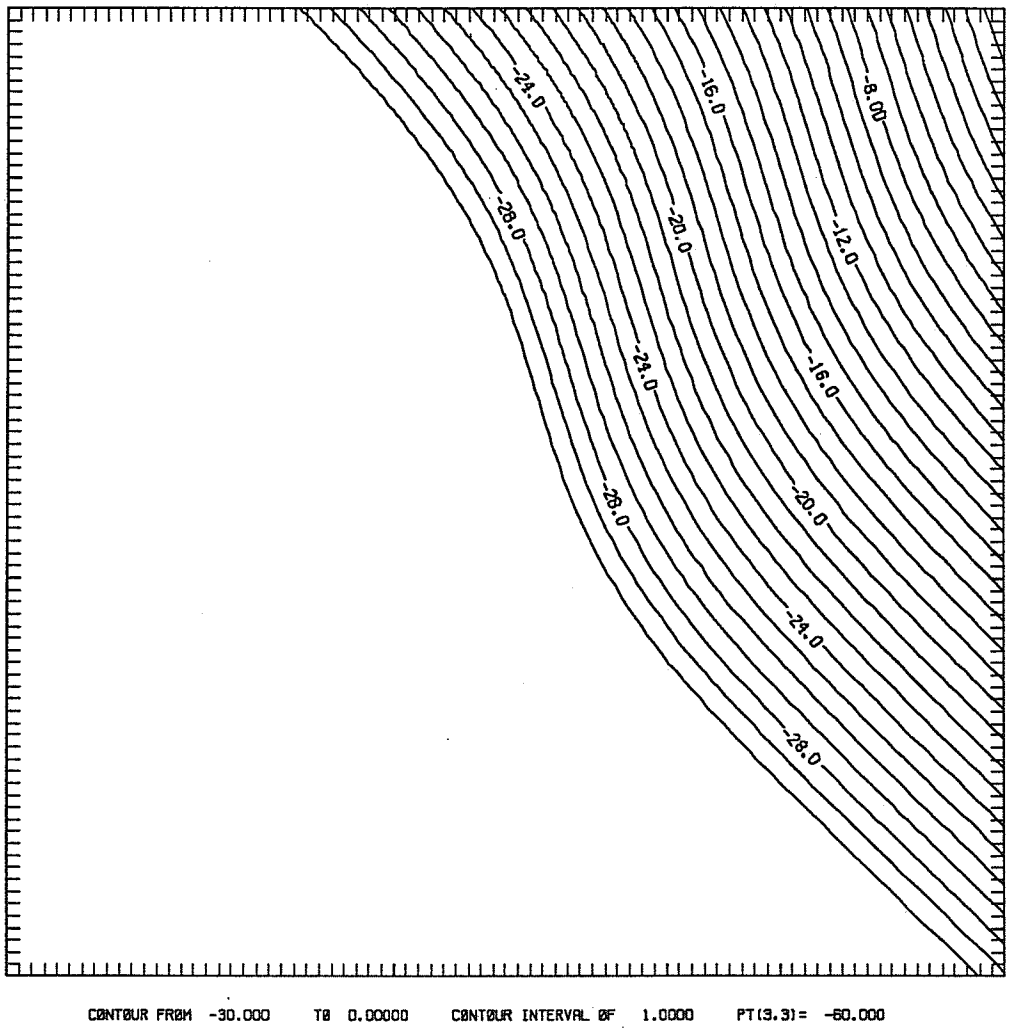

Figure B-3 Contour plot of the noise levels of the zener diodes using a worst-case analysis.

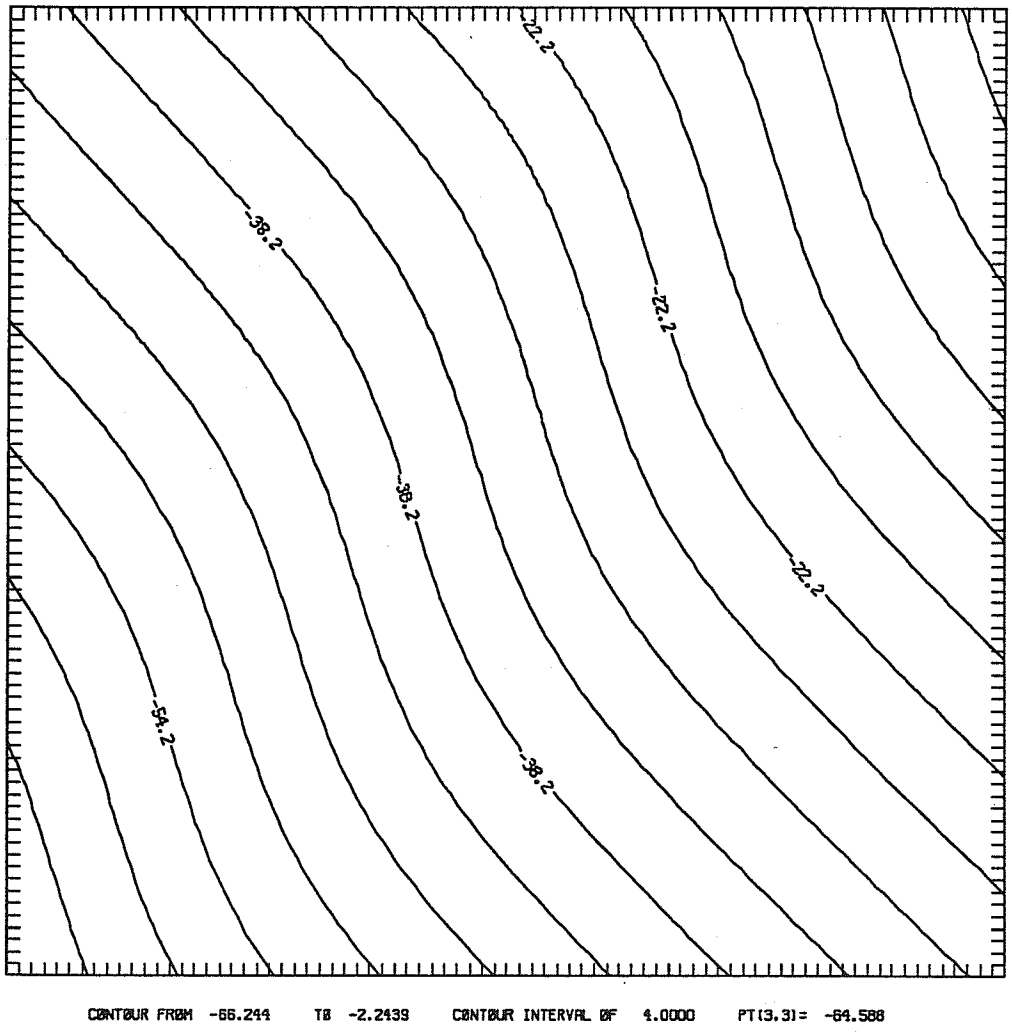

Figure B-4 Contour plot of the noise present within the current injection circuit.

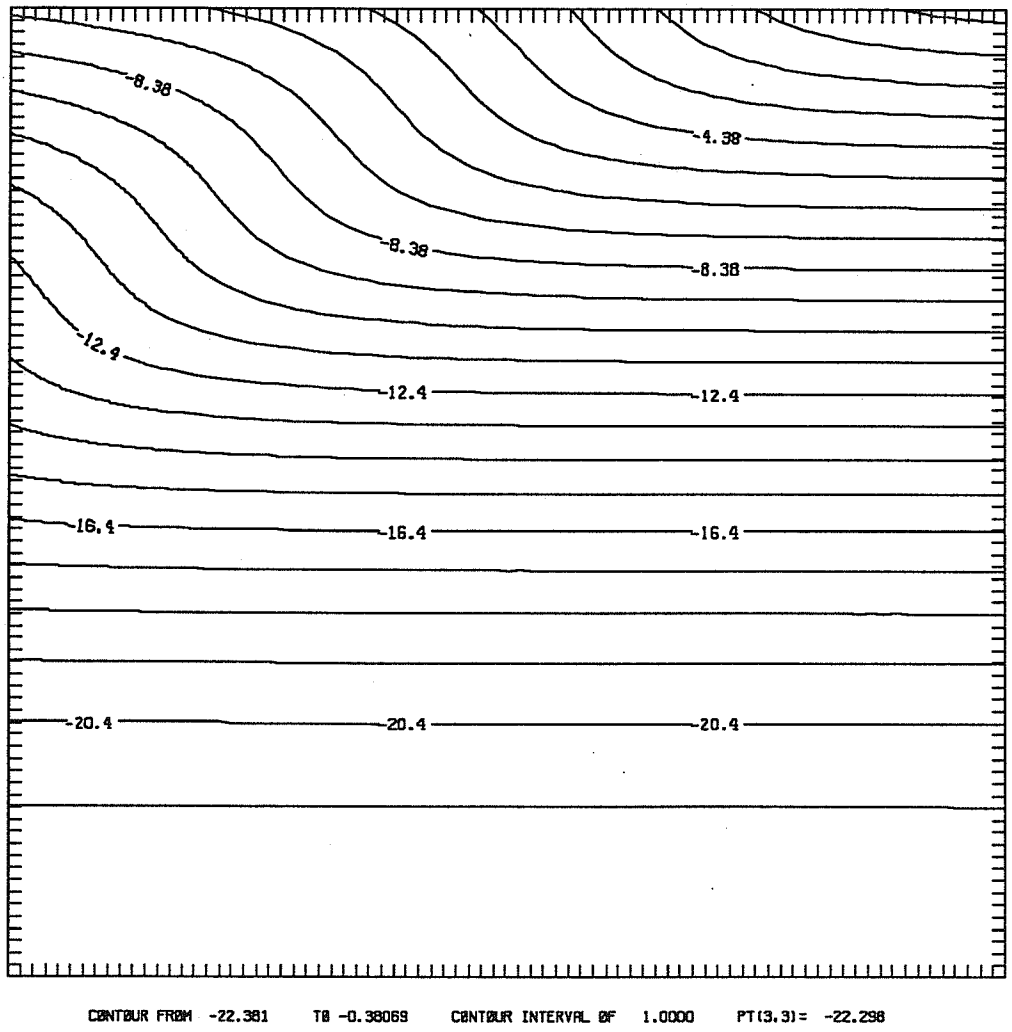

Figure B-5 Contour plot of the noise present at the output which is due to the input voltage noise of the operational amplifier.

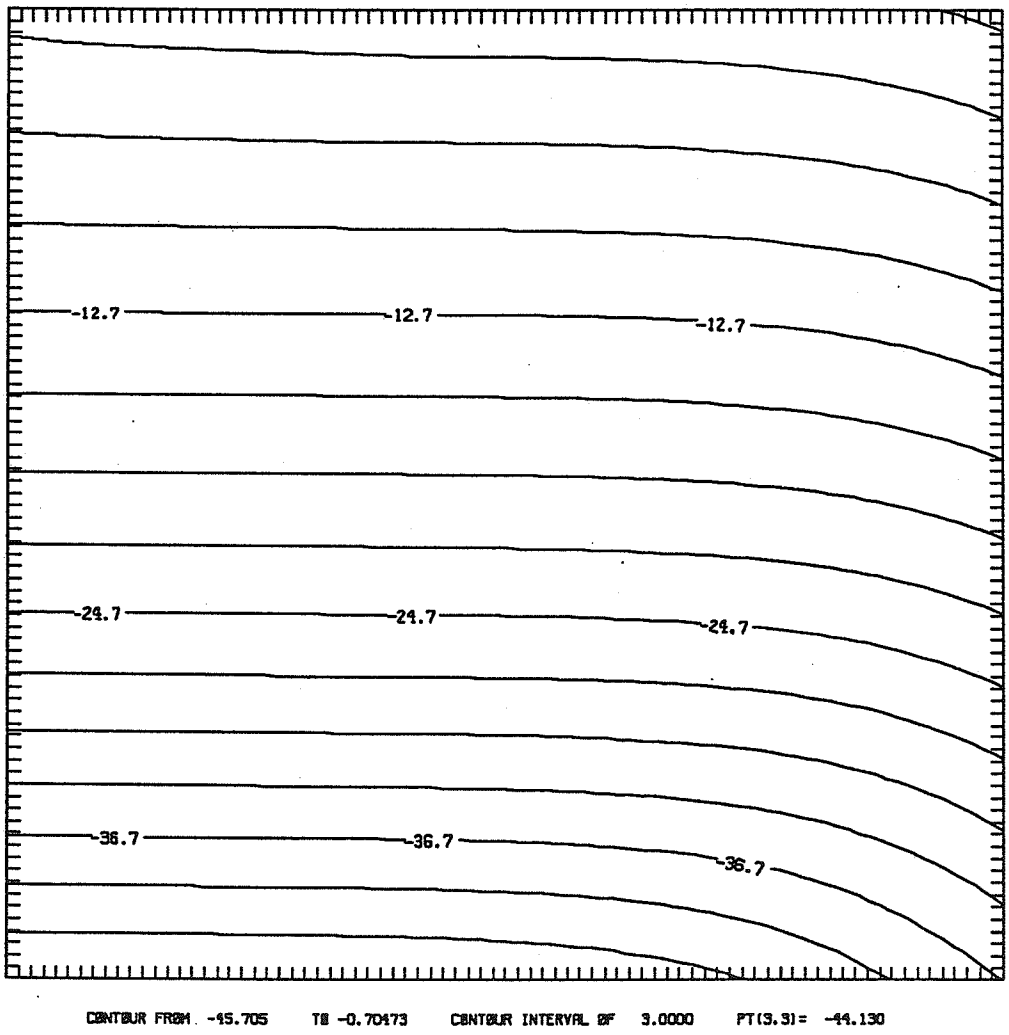

Figure B-6 Contour plot of the noise present at the output which is due to the input current noise of the operational amplifier.

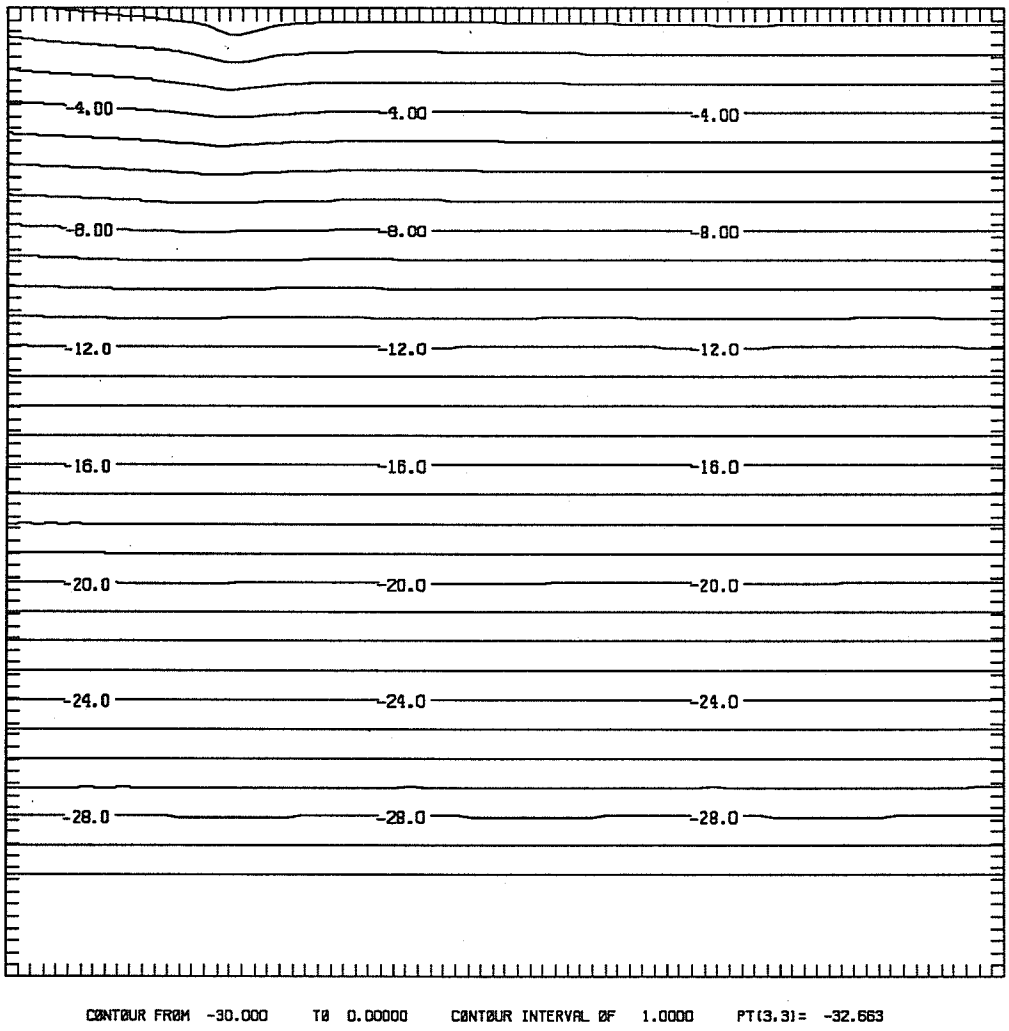

Figure B-7 Contour plot reflecting the noise levels at the output due to the Johnson noise of the feedback resistor.

Table B-3 The dB values corresponding to the total noise of the system.

Total noise of system	dB
1.5090E-03	-1.459
1.2072E-03	-3.397
9.6576E-04	-5.335
7.7261E-04	-7.274
6.1809E-04	-9.212
4.9447E-04	-11.15
3.9558E-04	-13.09
3.1646E-04	-15.03
2.5317E-04	-16.96
2.0253E-04	-18.90
1.6203E-04	-20.84
1.2962E-04	-22.78
1.0370E-04	-24.72
8.2958E-05	-26.66
6.6366E-05	-28.59
5.3093E-05	-30.53
4.2475E-05	-32.47

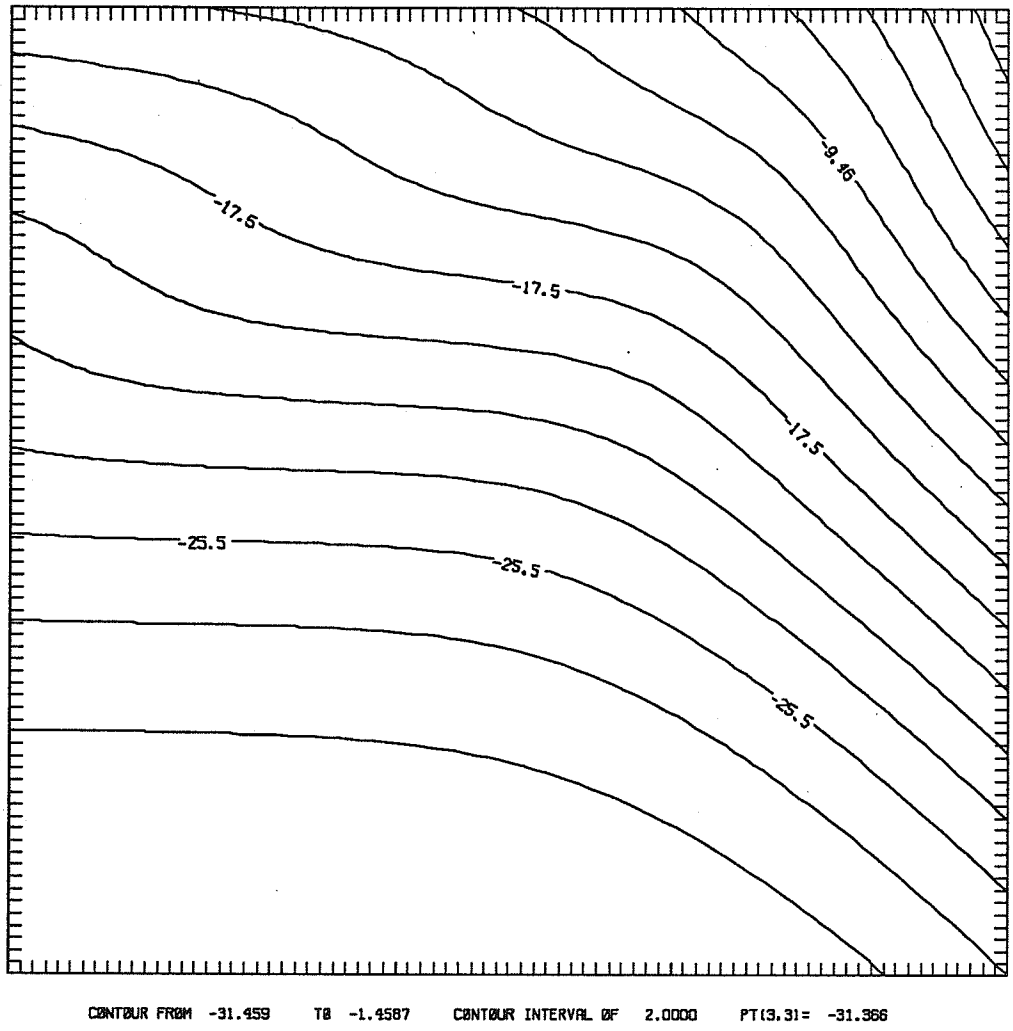

Figure B-8 Contour plot of the total output noise of the system; all noise elements are considered.

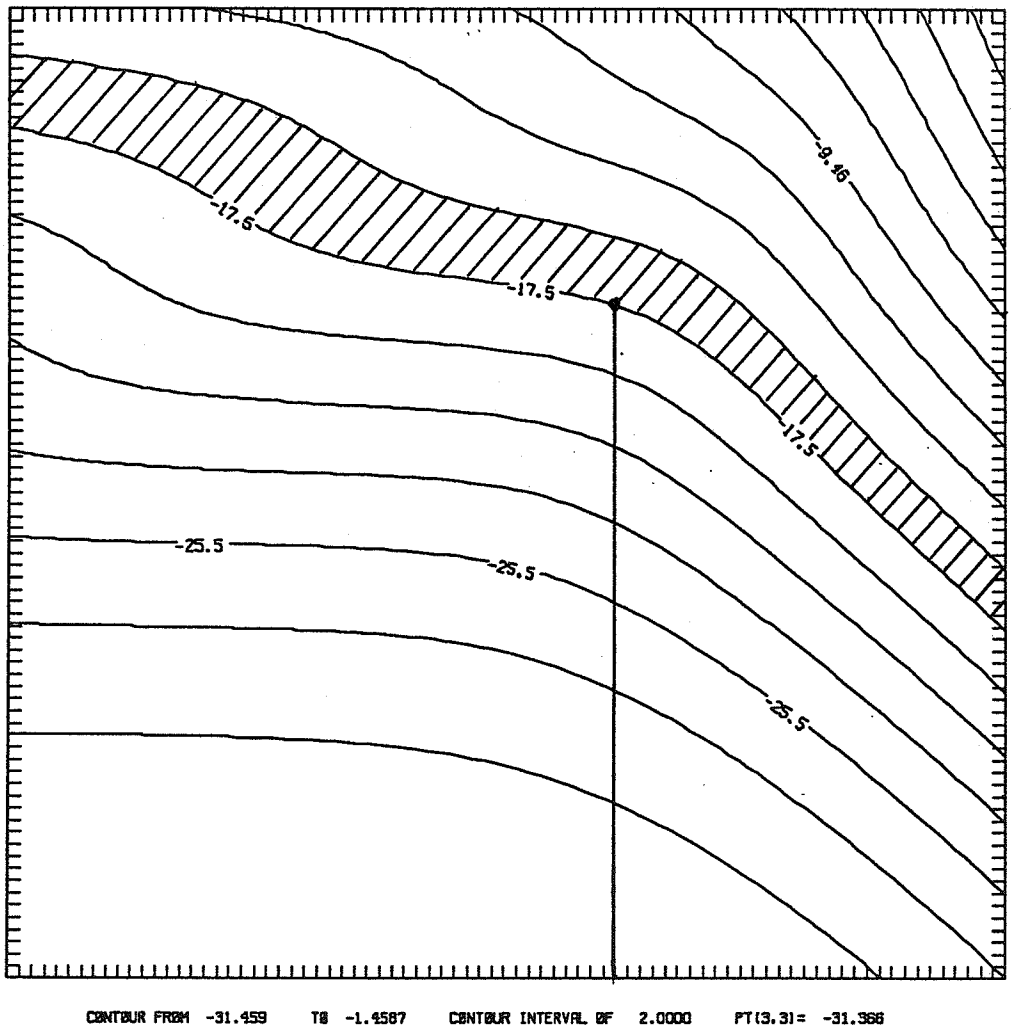

Figure B-9 Optimization technique used to choose the gain and the noise level of the system. The shaded area corresponds to the region on the plot with an acceptable noise level. The gain is then chosen as indicated by the solid line.

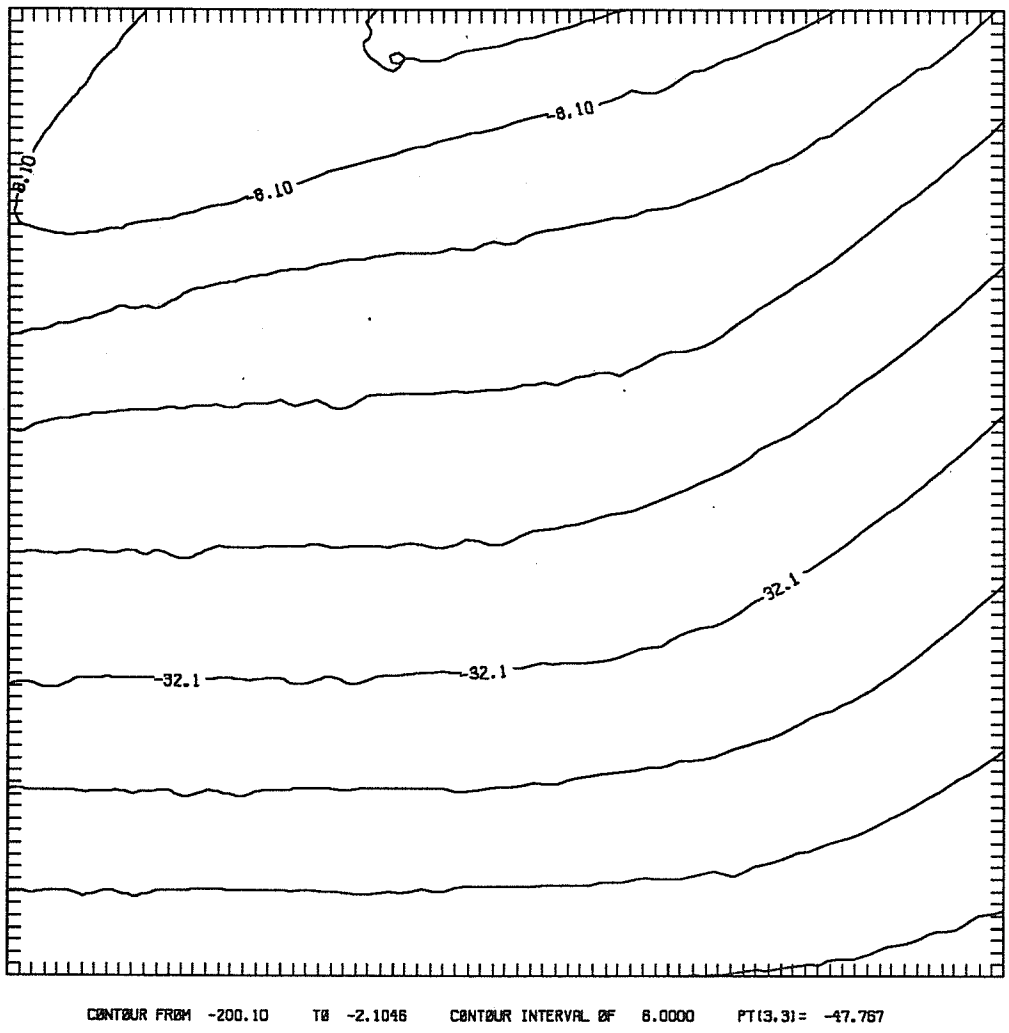

Figure B-10 Second noise optimization technique which maximizes the gain and the bandwidth while minimizing the noise.

APPENDIX C

COMPUTER PROGRAMS

Program #1 **Basic**

```
REM This program plots a number of the important frequency response
REM calculations for the amplifier-photodiode pair. These plots include:
REM
REM (1) open loop gain of the amplifier
REM (2) input noise voltage gain of the amplifier considering open loop
REM gain effects
REM (3) input noise voltage gain of the amplifier not considering open
REM loop gain effects
REM (4) input voltage noise spectral density
REM (5) input current noise spectral density
REM (6) transconductance gain of the amplifier
REM (7) output voltage noise due to input noise voltage
REM (8) output voltage noise due to input noise current
REM
LINE (10,10)-(10,260)
LINE (10,260)-(460,260)
READ rf,r1,c1,cf,ao,wo
a1=r1+rf
b1=r1*rf*cf+rf*r1*c1
g1=r1
n1=r1*rf*cf
a=b1
b=a1+b1*wo-ao*wo*n1
c=a1*wo-ao*wo*g1
LET d=b^2-(4*a*c)
IF d<0 THEN GOTO 20
p1=((-b+SQR(d))/(2*a))/6.283
p2=-((-b-SQR(d))/(2*a))/6.283
REM
REM calculate the values for the gain of the amplifier
REM
y1=260
z1=260
q1=260
l1=260
u1=260
v1=260
w1=260
t1=260
ze1=260
x1=10
x2=10
wzen=220000!
zno=9.3E-07
LET f=.0001
10 w=6.283*f
REM PRINT f
IF f=1E+11 THEN 100
re1=a1
im1=w*b1
```

```
re2=g1
im2=w*n1
d3=(re2^2)+(im2^2)
real=re1*re2+im1*im2
imag=im1*re2-re1*im2
mag=SQR(((real/d3)^2)+((imag/d3)^2))
phase=ATN(imag/real)
degr=INT(phase*57.295+.5)
db=INT((20*LOG(mag)+.5)/2.3)
y2=(260-db)
REM print f,db
LINE (x1,y1)-(x2,y2)
LINE (x1,270)-(x1,260)
IF f=100 THEN LINE (x1,270)-(x1,10)
REM
REM calculate the open loop gain of the amplifier
REM
re1=ao*wo
im1=0
re2=wo
im2=w
d3=(re2^2)+(im2^2)
real=re1*re2+im1*im2
imag=im1*re2-re1*im2
mag=SQR(((real/d3)^2)+((imag/d3)^2))
phase=ATN(imag/real)
degr=INT(phase*57.295+.5)
db=INT((20*LOG(mag)+.5)/2.3)
REM print db
z2=(260-db)
LINE (x1,z1)-(x2,z2)
15 REM
REM calculate the combined amplifier frequency response
REM
re1=a1*p1
im1=b1*w*p1
re2=g1*p1-n1*w^2
im2=g1*w+n1*p1*w
d3=(re2^2)+(im2^2)
real=re1*re2+im1*im2
imag=im1*re2-re1*im2
mag=SQR(((real/d3)^2)+((imag/d3)^2))
phase=ATN(imag/real)
degr=INT(phase*57.295+.5)
db=INT((20*LOG(mag)+.5)/2.3)
REM print db
q2=(260-db)
LINE (x1,q1)-(x2,q2)
REM
REM calculate the voltage noise spectral density of the op amp
REM
noise=8E-09
REM
REM p5 is the zero shown on the data sheet which
```

```
REM describes the noise spectral density of the opa101.
REM
p5=628
mag1=(noise/SQR(w))*(p5^2+w^2)^.25
phase=ATN(imag/real)
degr=INT(phase*57.295+.5)
db=INT((20*LOG(mag1)+.5)/2.3)
REM PRINT f,db,mag
l2=(20-db)
LINE (x1,l1)-(x2,l2)
REM
REM calculate the complete noise spectral density of the op amp
REM
re1=noise*p1*(a1*SQR(w)-b1*w^1.5+a1*SQR(p5*2))
im1=noise*p1*(a1*SQR(w)+b1*w^1.5+w*b1*SQR(p5*2))
re2=g1*p1*SQR(w)-(w^1.5)*(g1+n1*p1)-n1*w^2.5
im2=g1*p1*SQR(w)+(w^1.5)*(g1+n1*p1)-n1*w^2.5
d3=(re2^2)+(im2^2)
real=re1*re2+im1*im2
imag=im1*re2-re1*im2
mag=SQR(((real/d3)^2)+((imag/d3)^2))
mag2=mag1*p1*SQR(a1^2+(w*b1)^2)/(SQR((g1^2+(n1*w)^2)*(p1^2+w^2)))
phase=ATN(imag/real)
degr=INT(phase*57.295+.5)
db=INT((20*LOG(mag2)+.5)/2.3)
REM PRINT f,db,mag
u2=(40-db)
LINE (x1,u1)-(x2,u2)
REM
REM calculate the transconductance gain of the amplifier
REM
re1=-ao*r1*rf*wo
im1=0
de2=wo*rf+wo*ao*r1-w^2*rf*r1*c1-w^2*r1*rf*cf
dm2=w*wo*rf*r1*c1+w*wo*ao*r1*rf*cf+w*rf+w*r1
REM PRINT de2,dm2
d3=(de2^2)+(dm2^2)
real=re1*de2+im1*dm2
imag=im1*de2-re1*dm2
mag=SQR(((real/d3)^2)+((imag/d3)^2))
phase=ATN(imag/real)
degr=INT(phase*57.295+.5)
db=INT((20*LOG(mag)+.5)/2.3)
REM PRINT f,db,degr
v2=(260-db)
REM print f,db
LINE (x1,v1)-(x2,v2)
REM
REM calculate input the current noise of the amplifier.
REM
REM the noise current specified by the data is defined
inoise=1.4E-15
REM set the zero for the noise
z6=2*3.14159265#*10000
```

```
REM
re1=inoise
im1=w*inoise/z6
re2=1
im2=0
d3=(re2^2)+(im2^2)
real=re1*re2+im1*im2
imag=im1*re2-re1*im2
mag=SQR(((real/d3)^2)+((imag/d3)^2))
phase=ATN(imag/real)
degr=INT(phase*57.295+.5)
db=INT((20*LOG(mag)+.5)/2.3)
w2=(-60 -db)
REM print f,db
LINE (x1,w1)-(x2,w2)
REM
REM calculate the output noise voltage spectral density
REM due to the input noise current.
REM
k1=-ao*r1*rf*wo*inoise
REM
re1=k1
im1=k1*w/z6
re2=de2
im2=dm2
d3=(re2^2)+(im2^2)
real=re1*re2+im1*im2
imag=im1*re2-re1*im2
mag=SQR(((real/d3)^2)+((imag/d3)^2))
phase=ATN(imag/real)
degr=INT(phase*57.295+.5)
db=INT((20*LOG(mag)+.5)/2.3)
REM PRINT f,db
t2=(-50-db)
REM print f,db
LINE (x1,t1)-(x2,t2)
REM
REM determine the zener noise characteristics
REM
re1=-zno*w^2
im1=0
re2=wzen^2-w^2
im2=2*w*wzen
d3=(re2^2)+(im2^2)
real=re1*re2+im1*im2
imag=im1*re2-re1*im2
mag=SQR(((real/d3)^2)+((imag/d3)^2))
phase=ATN(imag/real)
degr=INT(phase*57.295+.5)
db=INT((20*LOG(mag)+.5)/2.3)
REM PRINT db
ze2=(-100-db)
REM PRINT f,db
LINE (x1,ze1)-(x2,ze2)
```

```
x1=x2
y1=y2
z1=z2
q1=q2
l1=l2
u1=u2
v1=v2
w1=w2
t1=t2
ze1=ze2
x2=x1+25
f=f*10
GOTO 10
20 REM print "error in quadratic - is imaginary"
100 REM near the end
REM print p1,p2
END
DATA 1e7
DATA 86.25e6
DATA 100e-12
DATA 1e-12
DATA 200000
DATA 500
```

Program #2 **Fortran**

```
c   This program calculates the total noise of the operational
c   amplifier-photodiode pair using integration techniques.
c
c
c   Set the variables for the analysis
c

      double precision r1,r2,r3,r4,r5,r6
      double precision vn1,vn2,vr3,vr4,ir5
      double precision rf,rp,cf,cp,Ao,wo
      double precision f,rad,git,dt,w
      double precision re1,re2,im1,im2
      double precision d3,re3,im3,trans,x4,x5,x3
      double precision wc1,wc2,filt
      double precision x,y,z,q,r,s
      double precision t,k,ft
      double precision a1,b1,g1,n1,inoise,k1,z6,p1,p5,vnoise,znoi,dark
      double precision vn3,vn4,in5,a,b,c,d,ioa
      integer m,n,i,fac,j,flg1,flg2
c
      double precision x6,x7,x8,x9,x10,x20,x21,x30
      double precision zener,eoa,ioa
      double precision john,shot,db3
c
c   Define the arrays
      dimension alpha(3,3)
c
c   set the constants
c
      cnt=0
      x=.5
c
c   Open the data file
      open (unit = 1, file = 'vals',status = 'old')
      open (unit = 3, file = 'noiseout', status = 'new')
c
c   Read the variables and constants from a data file
c
       read (1,*) r1,r2,r3,r4,r5,r6,rf,rp,cf,cp,Ao,wo,t,k,znoi,wc1,wc2,
     +vnoise,inoise,p5,z6,dark,e,ft
c
      write (3,*) r1,r2,r3,r4,r5,r6
      write (3,*) rf,rp,cf,cp,Ao,wo
      write (3,*) t,k,znoi,wc1,wc2
      write (3,*) vnoise,inoise,p5,z6
      write (3,*) dark,e,ft
      write (3,*) ' '
c
c   Set the beginning frequency and determine the divisions per decade
c   for the integration
c
```

```
c
      write (*,*) 'How many divisions per decade in the integration'
      read *,fac
      write (3,*) ' the potentiometer setting is at ',x
      write (3,*) ' the segments per decade for integration is ',fac
      write (3,*)
c     rf=100000
c     do 40 i=1,3
      cf=5.3e-12
c     do 30 j=1,3
      x1=0
      x2=0
      x3=0
      x4=0
      x5=0
      x6=0
      x7=0
      x8=0
      x9=0
      x21=0.50
      flg1=0
      flg2=0
      k1=-ao*rp*rf*wo*inoise
      a1=rp+rf
      b1=rp*rf*cf+rf*rp*cp
      g1=rp
      n1=rp*rf*cf
      a=b1
      b=a1+b1*wo-ao*wo*n1
      c=a1*wo-ao*wo*g1
      d=b**2-(4*a*c)
      if (d.lt.0) then
        write (*,*) 'error in quadratic'
        write (*,*) rf,cf
        d=-d
      end if
      p1=((-b+sqrt(d))/(2*a))/6.2832
      f=.001
      do 10 m=1,12
        rad=6.2831853*f
        dt=rad/fac
        do 8 n=1,(fac*10-fac+fac/2)
          w=rad+n*dt-dt/2
c
c         Calculate the complete output noise voltage due to the noise
c         spectral density of the operational amplifier.
c
          d3=(vnoise**2/w)*((p5**2+w**2)**x21)
          re3=p1**2*(a1**2+(w*b1)**2)
          im3=(g1**2+(n1*w)**2)*(p1**2+w**2)
          eoa=d3*re3/im3
          x6=x6+eoa*dt
c
c         Calculate the output noise voltage due to the input noise
```

```
c       current spectral density.
c
        re1=k1
        im1=k1*w/z6
        re2=wo*rf+wo*ao*rp-w**2*rf*rp*cp-w**2*rp*rf*cf
        im2=w*wo*rf*rp*cp+w*wo*ao*rp*rf*cf+w*rf+w*rp
        d3=(re2**2)+(im2**2)
        re3=re1*re2+im1*im2
        im3=im1*re2+im2*re1
        ioa=(((re3/d3)**2)+((im3/d3)**2))
        x7=x7+ioa*dt
c
c       calculate the transconductance gain of the amplifier
c
        re1=-Ao*rp*rf*wo
        im1=0
        re2=wo*rf+wo*Ao*rp-w**2*rf*rp*cp-w**2*rp*rf*cf
        im2=w*wo*rf*rp*cp+w*wo*Ao*rp*rf*cf+w*rf+w*rp
        d3=(re2**2)+(im2**2)
        re3=re1*re2
        im3=im2*re1
        trans=sqrt(((re3/d3)**2)+((im3/d3)**2))
c
c       Calculate the 3db down frequency (indicative of the frequency
c       response of the device).
c
        if (flg1.eq.0) then
          if (flg2.eq.0) then
            flg2=1
            db3=trans
          end if
          x30=db3/1.4142
          if (trans.lt.x30) then
            flg1=1
            x20=w/6.2831853
          end if
        end if
c
c       Calculate the noise due to the photodiode
c
        shot=2*e*dark*trans**2
        x8=x8+shot*dt
c
c       Calculate the Johnson noise due to the feedback resistor
c
        john=(4*k*t*trans**2)/rf
        x9=x9+john*dt
c
c       Calculate the noise due to different components in the
c       current injection circuit.
c
c
c       calculate the noise due to the zeners (worst-case calculation
c       since complete data for the noise was not given)
```

```
c
c
      zener=znoi/sqrt(ft)
c
c     Calculate the transfer function for the filter which limits
c     the zener voltages
c
      re1=wc2
      im1=0
      re2=wc2
      im2=w
      d3=(re2**2)+(im2**2)
      re3=re1*re2+im1*im2
      im3=im1*re2+im2*re1
      filt=sqrt(((re3/d3)**2)+((im3/d3)**2))
c
c     Calculate the zener noise
c
     vn1=((zener*filt)**2)*dt*trans**2
     r=(((1-x)*r6)*r5)/((1-x)*r6+r4+r5)
     s=r3+x*r6
     x1=x1+(vn1/r5)*(1-s/(s+r))
c
c
c
c
c     Calculate the noise voltage due to r3
c
     vn3=sqrt(4*k*t*r3)
     r=x*r6/r5
     s=x*r6/((1-x)*r6+r4)
     vr3=vn3/(r5*(1+s+r))
     x3=x3+(vr3**2)*dt*trans**2
c
c     Calculate the noise volatage due to r4
c
c
     vn4=sqrt(4*k*t*r4)
     r=(1-x)*r6/(r6*x+r3)
     s=(1-x)*r6/r5
     vr4=vn4/(r5*(1+s+r))
     x4=x4+(vr4**2)*dt*trans**2
c
c     Calculate the noise voltage due to r5
c
     ir5=(4*k*t/r5)
      x5=x5+(ir5*dt*trans**2)
c
8    continue
c
c
     x2=(2*x1+x3+x4+x5)
     x10=sqrt(x2+x6+x7+x8+x9)
    alpha(i,j)=x10
```

```
      write (3,*) 'frequency is ',f
      write (3,*) 'total noise is ',x10
      write (3,*) 'frequency response is ',x20
      write (3,*) 'current injection circuit noise is ',sqrt(x2)
      write (3,*) 'zener noise is ',sqrt(x1)
      write (3,*) 'johnson noise of r3 is ',sqrt(x3)
      write (3,*) 'johnson noise of r5 is ',sqrt(x5)
      write (3,*) 'voltage noise of op amp is ',sqrt(x6)
      write (3,*) 'current noise of op amp is ',sqrt(x7)
      write (3,*) 'shot noise is ',sqrt(x8)
      write (3,*) 'johnson feedback is ',sqrt(x9)
c
      f=f*10
c
c
10    continue
c
c
c
c     cf=cf/10
c
c30    continue
c
c     increment the value of r5
c
c     rf=rf*10
c
c40    continue
c
c     Print out the 2x2 matrix
c
      stop
      end
```

REFERENCES

[1]Peterson, J. I. , "Fiber optic chemical sensors - a view from past to the future," IEEE / NSF Symposium on Biosensors, pp. 35-39, September 1984.

[2]Seitz, W. R. , "Chemical sensors based on fiber optics," Analytic Chemistry, 56 (1): 16a-34a, 1984.

[3]Peterson, J. I. and Vurek, "Fiber optic sensors for biomedical applications," Science, vol. 224, pp. 123-127, 1984.

[4]Hahn, G.M. , "Hyperthermia: Background and Current Status," Luxtron Corperation Report, 1982.

[5]Freeman, J,E. and Hieftje G. M. , " A comparison of signal-to-noise ratios for near-infrared detectors," Applied Spectroscopy, volume 38, number 6, pp. 837-843 , 1984.

[6]DiDominico, M. and Svelto, O. , "Solid-state photodetection: A comparison between photodiodes and photoconductors," Proceedings of the IEEE, pp. 136-141, February 1964.

[7]Dereniak, E. L. , and Crowe D. G. , Optical Radiation Detectors, (John Wiley & Sons, Inc. , New York, 1984).

[8]Electro-optics Handbook, Technical series EOH-11, RCA Corporation, pp.160-172, (1974).

[9]McCarthy, J. F. and Magin, R. L. , "Development of a fiber optic pH and temperature sensing instrument," Whitaker Foundation Proposal, pp. 1-6, 1985.

[10]Douglas, Ross A. , Optoelectronic Devices and Optical Imaging Techniques, (Macmillan Press LTD. , London, pp. 31-67, 1979).

[11]Senturia, S. D. and Wedlock, B. D. , Electrical Circuit Analysis, (John Wiley & Sons, Inc. , New York, 1975).

[12]Yariv, A. , Introduction to Optical Electronics, (Holt, Rinehart, and Winston, New York, 1976).

[13]Helstrom, Carl W. , Probability and Stochastic Processes for Engineers, (Macmillan Publishing Company, New York, pp. 260-265, 1984).

[14]Silicon Photocells, T-1500, Hamamatsu Corporation, Japan, January 1985.

[15]Rectifiers and Zener Diodes: Motorola Data book, Motorola Inc. , 1982.

[16]Product Data Book, Burr Brown Corporation, 1984.